remote sensing

MDPI

Article

Benchmarking of Individual Tree Segmentation Methods in Mediterranean Forest Based on Point Clouds from Unmanned Aerial Vehicle Imagery and Low-Density Airborne Laser Scanning

Abderrahim Nemmaoui *, Fernando J. Aguilar and Manuel A. Aguilar

Department of Engineering, Research Centre CIAIMBITAL, University of Almería, Carretera de Sacramento s/n, La Cañada de San Urbano, 04120 Almería, Spain; faguilar@ual.es (F.J.A.); maguilar@ual.es (M.A.A.)
* Correspondence: an932@ual.es

Abstract: Three raster-based (RB) and one point cloud-based (PCB) algorithms were tested to segment individual Aleppo pine trees and extract their tree height (H) and crown diameter (CD) using two types of point clouds generated from two different techniques: (1) Low-Density (≈1.5 points/m^2) Airborne Laser Scanning (LD-ALS) and (2) photogrammetry based on high-resolution unmanned aerial vehicle (UAV) images. Through intensive experiments, it was concluded that the tested RB algorithms performed best in the case of UAV point clouds (F1-score > 80.57%, H Pearson's r > 0.97, and CD Pearson´s r > 0.73), while the PCB algorithm yielded the best results when working with LD-ALS point clouds (F1-score = 89.51%, H Pearson´s r = 0.94, and CD Pearson´s r = 0.57). The best set of algorithm parameters was applied to all plots, i.e., it was not optimized for each plot, in order to develop an automatic pipeline for mapping large areas of Mediterranean forests. In this case, tree detection and height estimation showed good results for both UAV and LD-ALS (F1-score > 85% and >76%, and H Pearson´s r > 0.96 and >0.93, respectively). However, very poor results were found when estimating crown diameter (CD Pearson´s r around 0.20 for both approaches).

Keywords: point clouds; forest inventory; individual tree detection; tree height; crown diameter; low-density ALS; UAV photogrammetry

check for updates

Citation: Nemmaoui, A.; Aguilar, F.J.; Aguilar, M.A. Benchmarking of Individual Tree Segmentation Methods in Mediterranean Forest Based on Point Clouds from Unmanned Aerial Vehicle Imagery and Low-Density Airborne Laser Scanning. *Remote Sens.* **2024**, *16*, 3974. https://doi.org/10.3390/rs16213974

Academic Editor: Brenden E. McNeil

Received: 30 September 2024
Revised: 20 October 2024
Accepted: 23 October 2024
Published: 25 October 2024

Copyright: © 2024 by the authors. Licensee MDPI, Basel, Switzerland. This article is an open access article distributed under the terms and conditions of the Creative Commons Attribution (CC BY) license (https://creativecommons.org/licenses/by/4.0/).

1. Introduction

Forests act as important carbon sinks and are, therefore, key components of the global carbon cycle. Accounting for carbon dioxide emissions is essential for assessing the effects of climate regulation policies as well as for understanding the services that forests provide to societies [1,2]. In this way, effective forest monitoring requires accurate and scientifically based data, being often conducted by teams of experts and fieldwork. However, these field surveys are uneconomical, time-consuming, exhausting, and not suitable for studies dealing with regular data collection [3].

Diameter at breast height (DBH) is one of the most important dendrometric measures in forest inventories. This parameter is widely used to estimate biomass, tree size distribution, basal area, tree volume, and aboveground biomass (AGB) at the plot or stand level. Various ground-based tools (e.g., calipers, Biltmore rods, and diameter tapes) [4] or laser scanning ground inventories [5] are commonly used to measure DBH. However, these techniques are labor-intensive, subjective, and time-consuming, especially when used over large areas [6,7]. Consequently, one of the key issues in forestry applications is to find an effective method to measure or estimate DBH over large areas [8].

In recent years, remote sensing (RS) has proven that it can provide independent, timely, and reliable forest information [9]. In this regard, forest monitoring using RS data has traditionally adopted an area-based approach to estimate summary forest statistics, such

as tree density (TD), growing stock, and stand height [10,11]. This approach is useful for large-area forest inventory and long-term management planning [12]. However, in the last two decades, a new tree-centric approach has emerged, based on the processing of point clouds to obtain individual trees (individual tree segmentation; ITS) and the automatic estimation of tree-level attributes (i.e., tree height, crown diameter, etc.) with high accuracy. In this way, it is necessary to highlight airborne laser scanning (ALS), which is considered one of the best techniques to produce point clouds from which to extract structural parameters of the forest [13–15]. Its main advantage is that this technology can penetrate vegetation and extract more vertical profile data compared to aerial images, even in low-light conditions [16]. This is the reason why ALS data have been used to estimate vertical forest structure for several applications, such as forest inventory [14], forest structure heterogeneity [17,18], fuel modeling and fuel type mapping [19], or tree damage detection after natural disasters [20].

Furthermore, advances in the use of unmanned aerial vehicle (UAV) technology and in data collection and processing have expanded the horizons of forest remote sensing and made the acquisition of high-resolution 3D data and orthoimages more readily available and affordable [8,21–26]. Using these technologies, end users can define spatial resolutions thanks to the availability of a wide range of sensors, providing great opportunities for forest managers [27,28]. Traditionally, these images were used to extract individual trees mainly through image segmentation within a 2D context, although nowadays UAV image-based approaches to derive high-density point clouds (3D information) are also frequently used in forest monitoring due to their higher throughput and low cost [29–32].

Many researchers have used a variety of approaches to extract individual tree parameters from 3D point clouds generated from ALS or UAV image data. These approaches, which allow the extraction of dendrometric features at the scale of individual trees, are alternative methods to the area-based approach (ABA) [33]. According to Koch et al. [34], these tree segmentation methods can be classified into (i) raster-based (RB), (ii) point cloud-based (PCB), and (iii) combined strategies (CS). RB strategies include the identification of local maxima (LM), region-growing (RG), valley-following (VF), and watershed approaches [35–39]. In general, all RB methods require less processing time than PCB methods because these types of algorithms must deal only with a single raster at a given resolution. In contrast, PCB methods focus on fully exploiting 3D data and do not transform the data into a raster [40], taking advantage of the space between the tops of individual trees to cluster points into a single tree based on proximity sampling rules and probable tree shape. To improve the extraction of individual trees, some strategies combined the strengths of the RB and PCB methods [41–44]. It is worth noting that state-of-the-art approaches use many parameters that need to be tuned to adapt the segmentation algorithm to a specific forest (i.e., local tuning). This parameter tuning is mostly done by adopting a trial-and-error approach [45], which is time-consuming and requires learning and understanding the meaning and role of each parameter.

Regarding tree detection accuracy, the first international comparative evaluation of the performance of different tree detection methods was conducted between 2005 and 2008 by the International Society for Photogrammetry and Remote Sensing (ISPRS), the European Spatial Data Research Organization (EuroSDR) and the Finnish Geodetic Institute (FGI). The results and conclusions of this study were published by Kaartinen et al. [46,47], highlighting mainly that the accuracy in the correct detection of trees ranged between 25% and 90% depending on the extraction method adopted.

Vauhkonen et al. [48] conducted another comparative study to test six different algorithms in different study areas and forest types located in Brazil, Germany, Norway, and Sweden. They concluded that the accuracy of tree detection was more influenced by the forest structure than by the selected algorithm. Following this research line, Eysn et al. [12] published in 2015 a new comparative study carried out in the Alpine Space. In this case, they applied eight methods, seven of which were based on the detection of LM in a raster Canopy Height Model (CHM), while the eighth method was a PCB method. They concluded that RB methods based on LM detection using variable-sized moving windows

were rated as the best-performing algorithm. More recently, Zaforemska et al. [49] evaluated up to five different tree segmentation algorithms (RB region-growing, local maxima centroidal Voronoi tessellation, PC-level region-growing, marker-controlled watershed, and continuously adaptive mean shift), with the latter method being rated as the most robust because it achieved a high level of accuracy in most reference plots without the need for extensive calibration.

Other studies have explored the effects of several variables on algorithm performance, for example, species-dependent structural parameters of individual trees or point cloud density [27,50–52]. Regarding point cloud density, Torresan et al. [52] and Kaartinen et al. [47] reported that high laser point density does not increase delineation accuracy, contradicting the results provided by Wang et al. [51] and Wallace et al. [27]. In fact, Torresan et al. [52] reported that tree segmentation accuracy was not affected when working with very high-density Lidar data (193 points/m^2) or medium/low-density data (8 points/m^2). Furthermore, Wang et al. [51] found that low-density ALS (LD-ALS) data (i.e., 2 points/m^2) provide satisfactory results when the goal of individual tree extraction is to measure only the dominant trees. In this sense, it is important to highlight that there are previous studies that have used LD-ALS data to estimate forest biomass [53–57], as well as tree height, crown diameter, basal area, stem density, and tree volume [35,58–65].

The main objective of this study is to test and compare the accuracy of individual tree detection, tree height, and crown diameter extraction from point cloud data derived from LD-ALS and UAV photogrammetry. As a secondary objective, a methodology requiring minimal user interaction will be developed for application in large areas of Mediterranean forests. The expected results should facilitate the production of large individual tree maps and the extraction of the corresponding dendrometric parameters from LD-ALS and UAV image data without spending time tuning algorithm parameters. To the best of the authors´ knowledge, this study is the first benchmark carried out for Mediterranean forests that provides the optimal sets of parameters for each tested algorithm.

2. Materials and Methods

2.1. Study Area

The work area was located in the Sierra de María-Los Vélez Natural Park (Figure 1), in the north of the province of Almería (Spain). Eighteen representative plots with 100 m sides (1 ha) were selected in the study area (Figure 1d), which mainly contain Aleppo pine (*Pinus halepensis* Mill.) as the dominant species (between 76% and 98%) with different percentages of vegetation cover ranging from 20% to 87%.

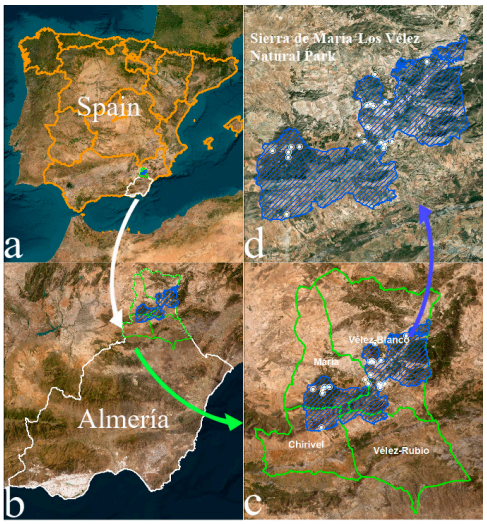


Figure 1. Location of the study area. (**a**) Province of Almeria (Spain) in white. (**b**) Region of "Los Vélez" (in green). (**c**) Sierra de María-Los Vélez Natural Park (in blue). (**d**) Reference field plots represented as white dots.

2.2. UAV Point Clouds

RGB images were taken between 4 and 8 March 2021, using a DJI Phantom 4 quadcopter UAV. Eighteen flight projects were scheduled and executed using the DJI Ground Station Pro app (SZ DJI Technology Co., Ltd., Shenzhen, China). Each mission was planned to cover one hectare (100 × 100 m^2). This hectare could include one, two, or up to three reference square subplots of 25 m on each side (Area of Interest; AoI).

According to Lin et al. [66], the selected flying height was 75 m above ground level. These authors studied the influence of different UAV flight altitudes on tree height estimation, reporting that the best accuracy was achieved flying at heights ranging from 60 m to 80 m. To avoid potential forest occlusions and improve individual tree detection, high forward and lateral overlaps of 90% and 85% were used [67].

Seven to eight ground control points (GCPs), consisting of rectangular artificial targets, were evenly distributed in each plot. The ETRS89 UTM 30N coordinates and the EGM08-REDNAP (Spanish High Precision Levelling Network) orthometric height of the center of each target were obtained using a GNSS RTK Reach RS2 (Emlid Ltd., St. Petersburg, Russia). The geographic coordinates of the base in each reference plot were obtained by applying the differential correction provided through an NTRIP caster from the continuous reference GPS station of Huercal-Overa (Andalusian GPS positioning network). Each base position was marked on the ground for subsequent reference data surveying (see Section 2.4. Reference Data—Ground Truth). The rover GPS receiver was used to measure the coordinates of each GCP in RTK mode using the base receiver as a reference.

Image processing was performed using the well-known SfM-MVS algorithm implemented in Agisoft Metashape Professional (V1.7.2) software (Agisoft LLC, Saint Petersburg, Russia) to generate 3 cm/pixel RGB orthoimages and dense UAV-based point clouds. GCPs collected in each reference plot were manually marked on the respective images to obtain the external orientation of each frame of the photogrammetric block, allowing georeferencing of point clouds and derived orthoimages in real-world coordinates.

The UAV point clouds were automatically classified into ground and non-ground points using the Adaptive Triangulated Irregular Network (ATIN) algorithm implemented in Metashape Professional [68]. Once the ground points in each 100 × 100 m^2 square plot were automatically labeled, the next step was the extraction of the 38 point cloud subsets as square reference plots within a 31 m side (i.e., AoI plus a 3 m buffer on each side). The choice of this length was made to avoid "edge effects" that would have resulted in the loss of data points belonging to trees at the edge. The final point cloud density represented an average of 2112.8 point/m^2, ranging from 1259.9 to 3237.7 point/m^2.

For each reference plot, a 0.5 m grid spacing Digital Terrain Model (DTM) was generated using the workflow proposed by Nemmaoui et al. [69]. By adopting this workflow, we can generate DTMs with a vertical bias lower than 10 cm, which is acceptable for forestry applications [70].

2.3. Low-Density Aerial Laser Scanner Data (LD-ALS)

The aerial laser scanner data used in this study were provided by the PNOA (National Plan of Aerial Orthophotography of Spain). These data were collected between 12 and 13 October 2020. The geodetic reference system was ETRS89 UTM Zone 30N, with orthometric heights referenced to the EGM08-REDNAP. They were acquired using the LEICA ALS80-HP (Heerbrugg, Switzerland) discrete return sensor with up to four returns. Data were provided in 2 × 2 km^2 mosaics of raw data points in LAS v.1.2 binary file format. The average point density was 1.5 points/m^2 (all returns), representing a nominal horizontal (at nadir) accuracy ($RMSE_{xy}$) and nominal vertical accuracy ($RMSE_z$) of less than 0.3 m and 0.15 m, respectively.

Considering that the classification of ground returns from the ALS point cloud is one of the most critical steps in the workflow [71,72], all LD-ALS point clouds were reclassified using the same algorithm previously applied in the case of UAV point clouds. The next step was the extraction of the 38 subsets (31 m × 31 m) of reclassified LD-ALS point clouds

corresponding to the reference plots. The final point cloud density took an average value of 3.5 point/m^2. For the normalization phase, a GMRF-DTM with 0.5 m grid spacing and free of outliers was also extracted for each reference plot.

2.4. Reference Data—Ground Truth

The field surveys in the 38 reference plots were conducted from 31 May to 11 June 2021. Each tree with DBH greater than or equal to 7.5 cm, and with tree height (H) greater than or equal to 2 m, was included in the inventory, with both species and health status (i.e., unharmed, broken, or dead). The ERTS89 coordinates of each tree were collected using the GNSS rover receiver Reach RS2 (RTK mode), allocating the GNSS base receiver in the positions marked on the ground during the UAV fieldwork campaign. Since errors related to tree location are another common source of individual tree detection errors [73], the extracted coordinates of the reference trees were verified using the 3 cm/pixel RGB UAV orthoimages. These orthoimages were also used to manually extract the crown diameters that were used as a reference for accuracy assessment. Tree height was also measured in each plot using a Nikon® Forestry Pro II rangefinder/hypsometer (Tokyo, Japan). The reference data can be considered homogenous due to the application of the same acquisition guidelines by the same experienced operators over all plots. The time lags between the fieldwork campaign and the acquisition of ALS and UAV data were 8 and 3 months, respectively. Despite this short time, it was verified that no significant changes took place in the study area in that period.

2.5. Processing and Workflow

Figure 2 provides an overview of the methodology and workflow adopted in this study. This workflow consists of four steps: (i) point cloud data normalization, (ii) input data generation (i.e., construction of CHM, smoothing CHM, detecting seeds or initial treetops (LM)), (iii) individual tree segmentation, and (iv) accuracy assessment for selecting the best parameters combination.

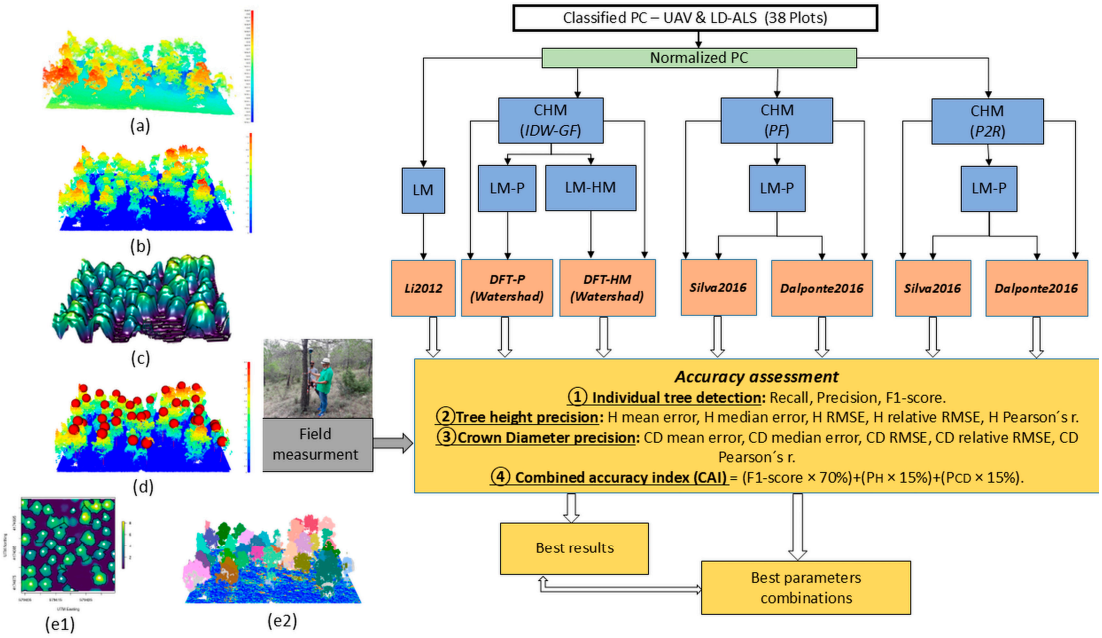


Figure 2. Workflow of the UAV and LD-ALS data processing, individual tree detection, accuracy assessment, and best parameters combinations. (**a**) Classified point cloud of the reference plot 16A1P; (**b**) normalized point cloud; (**c**) Canopy Height Model (CHM). (**d**) Normalized point cloud with seeds or treetops in red; (**e1**) 2D representation of the extracted parameters (position, height, crown diameter); (**e2**) 3D representation of the segmentation results.

2.5.1. Point Cloud Data Normalization

The GMRF-DTM with 50 cm grid spacing and free of outliers extracted from UAV and LD-ALS data were used to normalize the height of each point cloud corresponding to the 38 reference plots. The normalization process was performed by subtracting the corresponding terrain elevation (given by the DTM) from the Z value of each point. In this way, the original elevation of each point was replaced with its vertical height above the ground (Figure 2a,b) using the normalize_height function of the lidR package [74] implemented in R software (Version 1.4.1103) [75].

2.5.2. Construction of Canopy Height Models

The Canopy Height Model (CHM) can be seen as a surface, encoded as a raster image, which can be interpreted as a topographic map where local peaks indicate treetops (TT) and valleys bound tree crowns [36] (Figure 2c). Raster-based (RB) methods (i.e., CHM-based) are the most common and widely implemented nowadays for individual tree detection [76]. However, these methods force the point cloud data to be discretized into a grid. During this discretization process, information can be lost and errors introduced, especially for point clouds with a low point density [77], as is the case for the LD-ALS data used in this study. For this purpose, two different interpolation algorithms (point-to-raster and Pit-free) were tested to generate the CHM used as input for the Silva 2016 [39] and Dalponte 2016 [78] methods (see workflow depicted in Figure 2).

The point-to-raster (P2R) algorithm is one of the simplest and fastest algorithms used to generate a CHM [79,80]. This method consists of establishing a grid with a defined resolution and attributing to each pixel the elevation of the highest point. Applying P2R to low-density point clouds can have drawbacks. Some pixels may be empty if the resolution selected by the user is too fine for the available point density. This problem can be solved by applying post-processing to fill the gaps (e.g., interpolation) or by artificially densifying the point cloud. This artificial densification was the method adopted in this study when using LD-ALS data. This method was initially implemented in LAStools and consists of replacing each point in the original point cloud with a small circle of a user-specified diameter to simulate the fact that laser beams have a footprint [81]. This method was implemented into the software lidR package (Version 4.0.0). A 3×3 pixel mean smoothing filter was applied to all produced CHMs. This spatial window filter was selected because it was found to work well with trees that have irregular crown structures [39].

The Pit-free (PF) algorithm is a technique that exploits the 3D structure of tree canopies to remove existing height variations within point cloud data and resolve some issues associated with pits present in CHMs [82]. These pits are usually developed when the first return of ALS data is far below, which prevents the accurate extraction of forest parameters from the CHM [83,84]. The application of PF to normalized data and, in the case of LD-ALS data, to an artificially densified point cloud, involves two stages. The first stage includes constructing a standard CHM using all first returns and multiple CHMs from only those first returns related to higher-up vegetation hits. Once created, the next step consists of combining all the CHMs into one CHM where each cell location has the maximum value across all input rasters [82]. A 3×3 pixel mean smoothing filter was also applied to the produced CHMs. All these functions were implemented in R software.

The third preprocessing algorithm was the method implemented in the Digital Forestry Toolbox (DFT) [85] to build the corresponding CHM from the normalized point cloud. In this case, the Inverse Distance Weighted (IDW) interpolation method [86] was applied to obtain the raster CHM, in this case using a 3×3 pixel-smoothing Gaussian low-pass filter (GF) to the IDW-based CHM. Note that the DFT is executed as a Matlab script (MathWorks, Inc., Natick, MA, USA).

Finally, the smoothed CHMs were constructed with a spatial resolution of 0.25 m for UAV data and 0.5 m for LD-ALS data using the P2R, PF, and DFT-IDW algorithms.

2.5.3. Local Maxima Algorithm for Extracting Seed Points

The local maxima (LM) algorithm assumes that tree crowns (TTs) are represented by high local intensity maxima in the images. It uses two parameters: the smoothing window size (SWS) and the tree window size (TWS) [87]. Applying a smoothing filter helps eliminate spurious local maxima caused by spreading tree branches and twisted snags. The TWS parameter allows defining a fixed or variable limit within which the algorithm searches for the TT. In this sense, it is known that using fixed window sizes can lead to large commission and omission errors [88]. Wulder et al. [89] also reported that working with a variable window size (VWS) reduces both commission and omission errors.

In this study, the quadratic model proposed by Popescu et al. [90] in pine forests using only tree height (H) was adopted and applied as a circular shape (Equation (1)).

$$Crown\ width = 3.75105 - 0.17919H + 0.01241H^2 \quad (1)$$

This equation has been implemented into the LM function available in the LidR package in R [74]. This function includes a parameter that represents the minimum pixel height that can be considered as LM. In our case, this value was set to 2 m to avoid including TTs below 2 m, which is a standard technique to eliminate the effects of shrubs and ground points in the final segmentation [42]. The choice of this threshold was in accordance with the standard definition of forestry studies that specify that a tree of interest must reach a minimum height of 2 to 5 m [91].

2.5.4. Individual Tree Segmentation and Crown Delineation

Silva et al. (2016) [39] Approach (Silva 2016)

This region-growing algorithm [39] focuses on how to best approximate the intersection of multiple trees after locating the TTs or LM. In this study, the version written from scratch by the authors of the lidR package [74] was used. This version is based on a computation of a centroidal Voronoi tessellation [92] from the location of the input seeds. The seed is the center of the growing region, to which are added all those neighboring pixels that meet the conditions set by the fixed thresholds included in the function. The function and the corresponding parameters are defined in Table 1.

Table 1. Range of parameter values set in the segment_trees function to tune the Silva2016 algorithm applied to UAV and LD-ALS data. The Min and Max columns indicate the range of variation for the given parameter following the step indicated in the corresponding column.

	Definition and Threshold	Type	Measurement Unit	Min	Max	Step
Function	[(silva2016(chm, ttops, max_cr_factor = 0.6, exclusion = 0.3, ID = "treeID"))].	-	-	-	-	-
chm	Input raster layer. In this case, we used P2R and PF smoothed CHMs with 0.25 m and 0.5 m GSD for UAV and LD-ALS data, respectively (see method above).	Raster Layer	-	-	-	-
ttops	Spatial point data frame extracted using the LM function as described above.	Spatial Points Data Frame	-	-	-	-
max_cr_factor	Maximum value of a crown diameter given as a proportion of the tree height. Default is 0.6, meaning 60% of the tree height.	Numeric	-	0.1	0.9	0.1
exclusion	For each tree, pixels with an elevation lower than exclusion multiplied by the tree height will be removed. Thus, this number should be between 0 and 1.	Numeric	-	0.1	0.9	0.1
ID	Tree identification.	Character	-	-	-	-

Considering the tuning parameters described in Table 1 and those coming from CHM smoothing, we handled up to 162 combinations of segmentations for UAV data and 162 for

LD-ALS data. Once the 2D segmentation or labeling was done, it was transferred to the 3D point clouds (see Figure 2(e1,e2)) and then all metrics (i.e., tree positions, tree heights, and crown diameters) were extracted from each of the labeled trees.

Dalponte and Coomes (2016) [78] Approach (Dalponte2016)

This algorithm is also based on a seed/local maxima region-growing process [78], but applies a different strategy compared to Silva2016. In this case, regions grow from the seed by looking at intensity values rather than gravity distance. Unlabeled pixels are added to an adjacent region if the difference in intensities between the pixel and the LM is less than user-defined parameters [77]. The version of the algorithm written by the authors of the lidR package was used in this study. The function and corresponding parameters are defined in Table 2.

Table 2. Range of parameter values set in the segment_trees function to tune the Dalponte2016 algorithm applied to UAV and LD-ALS data. Those parameters with the symbol "#" in the step column were kept fixed, while the Min and Max columns indicate the range of variation for the given parameter following the step indicated in the corresponding column.

	Definition Threshold	Type	Measurement Unit	Min		Max		Step	
				UAV	LD-ALS	UAV	LD-ALS	UAV	LD-ALS
Function	[(dalponte2016(chm, ttops, th_tree = 2, th_seed = 0.45, th_cr = 0.55, max_cr = 10, ID = "treeID"))].	-	-	-	-	-	-	-	-
chm	Input raster layer. In this case, we used P2R and PF smoothed CHMs with 0.25 m and 0.5 m GSD for UAV and LD-ALS data, respectively (see method above).	Raster Layer	-	-	-	-	-	-	-
ttops	Spatial point data frame extracted using the LM function as described above.	Spatial Points Data Frame	-	-	-	-	-	-	-
th_tree	Threshold below which a pixel cannot be a tree. Default is 2.	Numeric	m	2	2	#	#	#	#
th_seed	Growing threshold 1. See reference in [78]. A pixel is added to a region if its height is greater than the tree height multiplied by this value. It should be between 0 and 1. Default is 0.45.	Numeric	-	0.1	0.1	0.9	0.9	0.1	0.1
th_cr	Growing threshold 2. See reference in [78]. A pixel is added to a region if its height is greater than the current mean height of the region multiplied by this value. It should be between 0 and 1. Default is 0.55.	Numeric	-	0.1	0.1	0.9	0.9	0.1	0.1
max_cr	Maximum value of the crown diameter of a detected tree (in pixels). Default is 10.	Numeric	pixels	10	2	100	16	10	2
ID	Tree identification.	Character	-	-	-	-	-	-	-

In this case, the number of segmentation outputs for each reference plot was 1620 for UAV and 1296 for LD-ALS data, respectively. For each combination, the segmentation was transferred from the 2D to the 3D point clouds. Subsequently, all metrics (i.e., tree positions, tree heights, and crown diameters) were extracted from the labeled point cloud.

Marker-Controlled Watershed Segmentation

The last RB algorithm tested was the marker-controlled watershed segmentation [7], which is included in the library Digital Forestry Toolbox (hereafter DFT) [85]. It is also a

region-growing algorithm that operates on topologically inverted data using the analogy of pouring water on seeds (TTs or LM) and considering basin boundaries as the water level [7,93]. Due to its practical suitability and logical evidence, this approach has been widely used to segment images for tree crown delineation [38]. The input CHM was produced using the IDW algorithm and a 3 × 3 pixel smoothing Gaussian filter (IDW-GF), as detailed before.

The approach adopted for seed extraction also consisted of using a variable window size [90]. This method was the simplest since no tuning parameters are needed. In this way, one output segmentation was obtained for each reference plot.

Li et al. (2012) [94] Approach (Li2012)

The Li 2012 algorithm [94] is a growing region approach that works directly with the 3D original point cloud. In this way, it was introduced into the field of individual tree detection (ITD) to overcome the limitations of raster-based approaches and take full advantage of 3D point cloud data [77]. It segments individual trees in a sequence considering the relative spacing between trees. It starts from the local maxima identified by the algorithm itself and "grows" a target tree, working at the raw point cloud level, including nearby candidate points and excluding points from other trees based on their relative spacing, starting the classification sequentially from the highest point to the lowest. This allows the algorithm to overcome the difficulty of classifying points at a lower level due to the lower spacing between trees.

As explained by Li et al. [94], points with spacing larger than a specified threshold are excluded from the target tree, while points with spacing smaller than the threshold are classified based on a minimum spacing rule. In this work, we used a strict implementation of this algorithm contained in the segment_trees function of the lidR package, to which the authors [74] added the minimum height parameter (i.e., "hmin" in the function, see Table 3). This addition was implemented to stop targeting objects that are too low (for more details, see https://rdrr.io/github/r-lidar/lidR/man/its_li2012.html, accessed on 2 February 2023). This parameter can be considered very useful because it avoids including shrubs and the lower layer of forest in the segmentation. However, this version is not parallelized (see https://rdrr.io/github/r-lidar/lidR/man/lidR-parallelism.html, accessed on 2 February 2023), and it is known to be slow because it has an algorithmic complexity worse than $O(N^2)$.

Table 3. Function and range of parameter values set to tune the Li2012 algorithm applied to UAV and LD-ALS point clouds. Those parameters with the symbol "#" in the step column were kept fixed, while Min and Max columns indicate the range of variation for the given parameter following the step indicated in the corresponding column.

	Definition Threshold	Type	Measurement Unit	Min		Max		Steps	
				UAV	LD-ALS	UAV	LD-ALS	UAV	LD-ALS
Function	[(li2012(dt1 = 1.5, dt2 = 2, R = 2, Zu = 15, hmin = 2, speed_up = 10))]	-	-	-	-	-	-	-	-
dt1	Threshold number 1. See reference on page 79 in [94]. Default is 1.5.	Numeric	m	1.4	1.4	1.6	2	0.1	0.2
dt2	Threshold number 2. See reference on page 79 in [94]. Default is 2.	Numeric	m	2	2	2.3	3	0.1	0.2
R	Search radius. See page 79 in [94]. Default is 2.	Numeric	m	1	1	5	9	1	1
Zu	If point elevation was greater than Zu, dt2 was used, otherwise dt1 was used. See page 79 in [94]. Default is 15.	Numeric	m	15	15	#	#	#	#
hmin	Minimum height of a detected tree. Default is 2.	Numeric	m	2	2	#	#	#	#
Speed-up	Maximum radius of a crown [94]. Default is 10.	Numeric	m	5	5	#	20	#	5

A parameter tuning procedure similar to that used to tune the RB algorithms was applied, varying the value of the parameters of Li2012 in the ranges reported in Table 3. Considering all the combinations for the tuning parameters, the sum of the segmentation outputs for each reference plot was 60 for UAV and 864 for LD-ALS data, respectively.

2.5.5. Accuracy Assessment: Tree Detection and Dendrometric Feature Estimation

The typical approach used to match the segmented tree with the field-controlled tree is the one developed by Dalponte and Coomes [78]. According to this approach, if only one field-measured tree is included within a delineated crown, this tree is associated with the corresponding segmented tree. Otherwise, if more than one field-measured tree is included in a segmented crown, the field-measured tree with the height closest to the height of the segmented tree is chosen. However, as seen in the results of this study, some algorithms (especially Li2012) delineate much larger crowns than exist in reality. In fact, as the delineated crown has a large diameter, there are always different field-measured trees within the crown obtained, and this effect increases the error of the result. Torresan et al. [52] reported that adopting this matching method may lead to a low tree detection rate.

Eysn et al. [12] proposed another tree-matching approach. If multiple reference trees match the same segmented tree, only the one with the shortest 2D distance and shortest height difference is matched. Other methods also consider the planar distance between delineated and reference trees (e.g., [95]), 2D Euclidean Distance (e.g., [27,48]), or the maximum values of height differences (e.g., [48,96]).

In this study, a fully automated tree-matching procedure was developed and applied through a Matlab script to link the different detected trees and the corresponding extracted ones. Compared to a traditional human interpretation (e.g., [39]), this methodology allows for a clear, reproducible, and objective test. Considering that when applying all parameter combinations, more than 158,308 results (i.e., 4166 combinations applied to the 38 reference plots) should be compared manually, this automatic method was very useful. The automatic accuracy assessment took a few seconds per plot and the results indicate that the matching procedure worked well.

The input data for this automated tree matching were the field inventory (FI) collected as detailed before in Section 2.4. The matching procedure was performed in three general steps:

(i). First, all input data within an AoI (i.e., the 25 × 25 m^2 reference plots) were selected for the matching procedure. For a test tree, the closest neighbor reference tree within a 2D Euclidean Distance of 2 m was matched. This approach is similar to that adopted by other authors [27,48]. Additionally, the already assigned neighbor reference tree cannot become a candidate to match another extracted tree. Our distance matching threshold was generally similar, or even more conservative, than that used in previous studies (e.g., 4 m [97], 3 m [98], and between 3 and 5 m [12]).

(ii). In field inventory, tree location is usually measured at the bottom of the stem, while the position of the segmented tree corresponds to the highest point (i.e., TT). If the tree shows a curved stem or it is located on a steep slope, the location of the TT and the bottom of the stem differ. This effect increases with increasing tree height [12]. This distance can cause confusion and, above all, increase errors in trees located on the edge. In other words, due to the displacement indicated above, there are trees whose trunks are actually on the edge, but the highest point is projected outside the AoI. Thus, once the trees were paired following the first step detailed above, any possible conflicts between the trees located on the boundaries were resolved. For this, several situations were considered: (a) The reference tree is outside the AoI. In this case, this tree is removed from the ground truth, together with the matched extracted tree, if any. (b) If the segmented tree is outside the AoI and does not match, it is automatically deleted. If it matches a reference tree located in the AoI, it is preserved.

(iii). Once the final set of reference and segmented trees were selected, the Euclidean Distance was calculated again, and all matching pairs are compared before tackling the step of calculating the statistical parameters for the accuracy assessment. The results of the automatic comparison were validated by visual interpretation by an experienced human interpreter.

Accuracy assessment was performed in terms of statistical measures as follows:

(a) Accuracy of tree detection and segmentation. Tree detection was evaluated in terms of recall, precision, and F1-score. Recall (r) (Equation (2)) denotes the measurement of the detected trees, and it is inversely related to omission error or under-segmentation error. Precision (p) (Equation (3)) gives a measure of the trees detected correctly and it is inversely related to commission error or over-segmentation error. F1-score (Equation (4)) is given by the harmonic mean of recall and precision. The values of r, p, and F1-score were calculated as percentages. The higher the values, the better the tree segmentation accuracy. These metrics have been used in several studies [39,94,99,100].

$$r = \frac{TP}{(TP + FN)} \times 100 \quad (2)$$

$$p = \frac{TP}{(TP + FP)} \times 100 \quad (3)$$

$$F1 - score = \frac{2 \times r \times p}{(r + p)} \times 100 \quad (4)$$

[TP or True positive is a field tree that matches an extracted tree (correct detection); FN or False negative means that a field tree is not matched (omission error); FP or False positive is accounted if an extracted tree does not have any matched tree from the field data (commission error)].

(b) Accuracy of tree height estimation (H). Tree height accuracy was assessed by applying some error statistics to each matched tree and comparing its H, estimated value (i.e., automatically extracted) and H_{FI}, observed value (i.e., FI) through their difference, H-H_{FI}. The selected metrics included mean error and median error (systematic error). Due to its wide use, the H root mean square error (H RMSE) was also calculated. In addition, the relative H RMSE was computed by dividing the RMSE by the mean H value observed in the reference plot in order to intuitively scale the magnitude of the random error. The Pearson's coefficient of linear correlation between estimated and observed values was also calculated.

(c) Accuracy of crown diameter (CD) estimation. It was evaluated by comparing the crown diameter extracted by each algorithm with the reference diameter manually digitized over the 3 cm/pixel UAV-based orthoimage. The statistical parameters calculated were similar to those obtained in the case of calculating the accuracy in estimating tree height. In that sense, CD mean error, CD median error, CD RMSE, CD relative RMSE, and CD Pearson´s r were determined.

In this study, it has been considered that each algorithm must comply with the following goals: (i) identifying the maximum number of trees existing in each AoI and (ii) extracting the height and crown diameter of each tree with the highest possible accuracy. For this reason, a combined accuracy index (CAI) (Equation (5)) ranging from 0 to 100% was introduced to weight the importance of each objective. The first step, tree detection, is the most critical and should have the highest importance (i.e., 70% of the weight). Once the trees have been correctly detected, the goal is to determine the dendrometric parameters (H and CD) of each tree. Equation (5) shows the weight attributed to each objective:

$$CAI = (F1 - score \times 70\%) + (P_H \times 15\%) + (P_{CD} \times 15\%) \quad (5)$$

[F1-score is given by Equation (4), but ranges from 0 to 1 in this case; P_H and P_{CD} are the Pearson's coefficients of linear correlation (ranging from 0 to 1) corresponding to tree height and crown diameter, respectively].

To select the best-performing ITD parameter set for each algorithm tested in this study, the accuracy results were first evaluated. The set of parameters that most frequently yielded the best results were selected and applied to all plots. This second round of algorithm testing was intended to evaluate the accuracy produced by each algorithm by applying the same parameters to all reference plots, thus resembling the accuracy obtained if an ITD algorithm were applied to a large area.

3. Results

3.1. Characteristics of the Reference Plots

Table 4 presents the most important dasometric characteristics of the 38 AoIs. These include vegetation cover provided by trees taller than 2 m, tree density per hectare, tree heights, and the plot-level uniformity index (PH^350 in Equation (6), which is an indicator to estimate the variability in tree growth rates [87]). Plots that have a PH^350 index in the range of 0.37 to 0.50 are considered homogeneous plots from the point of view of the height of the trees they contain. Basal area (G) and Lorey´s mean height (Lh) were also calculated for each AoI.

$$PH^350 = \frac{\sum_{i=1}^{n/2} H_i^3}{\sum_{i=1}^{n} H_i^3} \quad (6)$$

Table 4. Characteristics of the 38 AoIs (above 2 m height vegetation cover (VC), density (D), tree height (H), plot-level uniformity index (PH350), basal area (G), and Lorey's height (Lh)) (1): standard deviation.

Plot Name	VC (%)	D (Trees/ha)	Tree Height (H) (m)				PH^350	G (m^2/ha)	Lh (m)
			Average H (m)	Max H (m)	Min H (m)	sd H (m) (1)			
1B21P	30.22	224	4.90	6.22	3.30	0.93	0.30	5.97	5.30
1B22P	30.22	448	3.02	4.37	2.26	0.54	0.29	1.52	3.48
1B32P	29.17	320	3.22	4.35	2.03	0.68	0.27	2.01	3.68
3A2P	21.08	128	7.46	10.20	4.66	2.35	0.21	8.04	9.16
3A3P	26.46	128	8.75	13.16	3.69	3.54	0.15	12.71	11.26
4B1P	31.98	144	12.07	15.37	4.30	4.44	0.31	17.00	14.31
4B 2P	28.67	160	8.77	15.93	3.10	5.88	0.01	11.99	15.15
4B 4P	50.22	208	12.08	16.03	5.17	2.71	0.31	18.51	13.14
5A1P	31.09	144	12.01	14.05	7.50	1.89	**0.37**	15.64	12.75
6A1P	50.81	256	12.96	15.24	11.31	1.07	**0.41**	21.73	13.24
6A2P	59.27	224	13.84	15.61	10.67	1.39	**0.39**	26.46	14.02
6A3P	60.56	352	10.47	13.48	3.40	2.32	0.30	25.99	11.47
7A1P	38.03	128	13.93	18.66	4.90	4.45	0.26	19.95	16.21
7A2P	19.99	96	12.57	17.04	8.36	3.44	0.19	9.32	14.94
7A3P	36.34	176	14.00	15.10	12.08	0.87	**0.44**	19.74	14.10
8A1P	33.43	192	8.25	11.03	2.90	2.62	0.29	13.14	9.51
8A2P	43.00	336	7.23	9.21	5.54	1.04	0.34	17.41	7.49
8A3P	42.58	224	9.14	10.53	7.19	0.91	**0.39**	16.72	9.32
10A1P	57.92	640	7.11	9.38	2.20	1.44	0.34	22.96	7.51
10B1P	48.35	288	10.28	12.13	7.64	1.16	**0.38**	23.91	10.60
10B2P	24.36	128	11.59	13.62	9.20	1.40	**0.39**	14.40	12.03
10B4P	60.36	416	10.94	14.11	6.73	1.49	0.35	30.20	11.43
12A1P	66.74	864	7.95	10.63	5.38	1.24	0.32	30.14	8.40
12A2P	62.51	944	6.84	10.05	2.71	1.50	0.27	23.88	7.33
12A3P	67.86	608	8.80	13.62	2.10	3.03	0.18	32.38	10.99
13A1P	34.97	368	4.82	7.71	2.70	1.25	0.24	7.75	5.55
13A3P	38.83	336	5.90	8.44	3.08	1.37	0.27	9.71	6.65
13B1P	54.33	288	9.95	11.08	8.39	0.74	**0.42**	22.22	10.04
13B2P	48.72	416	9.52	11.39	5.75	1.12	**0.40**	22.82	9.71
13B3P	41.19	256	9.72	13.06	4.48	2.17	0.30	18.86	10.58
13B4P	25.92	176	6.39	9.69	2.50	2.91	0.09	8.61	8.91
14A1P	59.67	336	9.30	11.25	6.69	1.29	0.35	26.66	9.54
14A3P	66.70	368	8.89	11.30	4.45	1.31	**0.37**	27.29	9.00
16A1P	50.49	592	6.08	8.37	3.67	1.09	0.30	14.74	6.43

Table 4. *Cont.*

Plot Name	VC (%)	D (Trees/ha)	Tree Height (H) (m)				$PH^3$50	G (m^2/ha)	Lh (m)
			Average H (m)	Max H (m)	Min H (m)	sd H (m) (1)			
16A2P	53.40	448	6.32	8.59	3.77	1.26	0.30	15.66	6.55
17A3P	86.79	1504	8.74	11.56	4.00	1.38	0.34	36.03	9.13
18A1P	66.91	544	6.97	9.29	3.84	1.20	0.30	26.31	7.44
18A3P	41.69	704	5.54	7.56	3.60	0.95	0.31	19.38	5.79
Max	86.79	1504.00	14.00	18.66	12.08	5.88	0.44	36.03	16.21
Min	19.99	96.00	3.02	4.35	2.03	0.54	0.01	1.52	3.48
Average	45.29	371.37	8.85	11.54	5.14	1.85	0.30	18.36	9.79

Vegetation cover had an average value of 45.29% (ranging from 19.99% to 86.79%), while basal area values ranged from 1.52 to 36.03 m^2/ha (average 18.36 m^2/ha). Lorey's mean height had an average of 9.79 m, with a range from 3.48 m to 16.21 m. The 38 selected AoIs had an average tree density of 371.37 trees/ha (ranging from 96 trees/ha to 1504 trees/ha). Regarding the homogeneity of tree height within the reference plots estimated from the $PH^3$50 index, 10 AoIs (in bold in Table 4) can be considered homogeneous.

These plot-level parameters reflect the dominance in each plot of the upper, lower, or both canopy layers. Some plots, especially those situated in the most humid areas of the park, are representative of a very unique and interesting ecosystem made up of a mixture of dominant pine trees and understory vegetation mainly formed by small holm oak trees (*Quercus ilex* L.) [69]. This lower canopy layer and stratification effect have a visible effect on estimating tree heights [52]. It is necessary to highlight that the omission error is usually higher for multi-layered coniferous and mixed forest areas compared to the single-layer coniferous forest areas [12].

3.2. Tree Detection Accuracy

Table 5 shows the recall, precision, and F1-score of each algorithm using UAV and LD-ALS data. For all algorithms, the accuracies in terms of the F1-score obtained are above 86% and 75% for the UAV and LD-ALS data, respectively.

Table 5. Tree detection accuracy for the four tested algorithms using UAV and LD-ALS data in terms of average values of accuracy metrics for all reference plots.

Algorithm	CHM	UAV			LD-ALS		
		Recall	Precision	F1-Score	Recall	Precision	F1-Score
Silva2016	Best of P2R-MF and PF-MF	84.45	99.00	90.47	74.76	97.95	83.54
	P2R-MF	84.02	98.75	90.13	74.18	97.94	83.13
	PF-MF	82.77	98.54	89.22	72.64	97.87	81.92
Dalponte2016	Best of P2R-MF and PF-MF	82.56	96.75	88.38	72.72	96.26	81.60
	P2R-MF	81.68	96.19	87.60	72.12	95.77	80.96
	PF-MF	80.57	96.03	86.87	70.78	95.56	79.84
DFT	IDW-GF	85.67	96.36	90.02	78.67	76.41	75.66
Li2012	-	82.95	94.00	86.99	86.08	94.32	89.51

In the case of UAV data, the algorithm that achieved the best results was Silva2016. After proper adjustment of its tuning parameters and the input CHM (the best of P2R-CHM and PF-CHM), it achieved an average F1-score of 90.47%. Very similar values were obtained when P2R-CHM or PF-CHM were applied to all reference plots, obtaining F1-score values of 90.13% and 89.22%, respectively. The DFT algorithm yielded tree detection rates very similar to those obtained using the Silva2016 algorithm, with an F1-score of 90.02%. It should be noted that this method has the great advantage of not having to tune any parameter because it only works with a single option. The Dalponte2016 algorithm was ranked third, with F1-score values ranging from 86.87% to 88.38%. The best results were achieved when both the algorithm parameters and the input CHM were adjusted. When

choosing to work with only one input CHM, the CHM generated with the P2R method performed slightly better, reaching an average F1-score value of 87.60%.

Also, as regards the results of the UAV data, the only algorithm that works directly with point clouds was the one that gave the worst results. In this case, the accuracy obtained in terms of F1-score was 86.99%.

With respect to LD-ALS data, the best accuracy in terms of F1-score was obtained using the Li2012 PCB algorithm, reaching an average F1-score of 89.51%. The order of the RB algorithms, in terms of F1-score accuracy, was similar to that obtained when working with UAV data. Silva2016 was the best (83.54%), followed by Dalponte2016 (81.60%), and DFT (75.66%). In the case of the Silva2016 and Dalponte2016 algorithms, and when comparing the two methods tested in this study to generate the input CHM, it was observed that, in general, the P2R algorithm provided better results.

Importantly, regardless of the algorithm and type of point cloud acquisition (UAV or LD-ALS), the precision metric remained higher than the recall, indicating that the algorithms used in this study tended to miss some trees (omission error). This effect was more marked with the LD-ALS data.

Figure 3 shows the box-and-whisker plots (variability in accuracy due to parameter tuning), along with the histogram in the case of the DFT method (no tuning), in relation to the individual tree detection accuracy (F1-score) of the algorithms tested on both UAV and LD-ALS point clouds. The 38 reference plots (X-axis) are represented in ascending order of vegetation cover (see Table 4). In each box, the center mark indicates the corresponding median value, and the lower and upper ends of the box indicate the 25th and 75th percentiles, respectively. Whiskers extend to the most extreme data points not considered outliers, representing 1.5 times the interquartile range (IQR). Outliers are represented individually by the "+" markers (symbol in red).

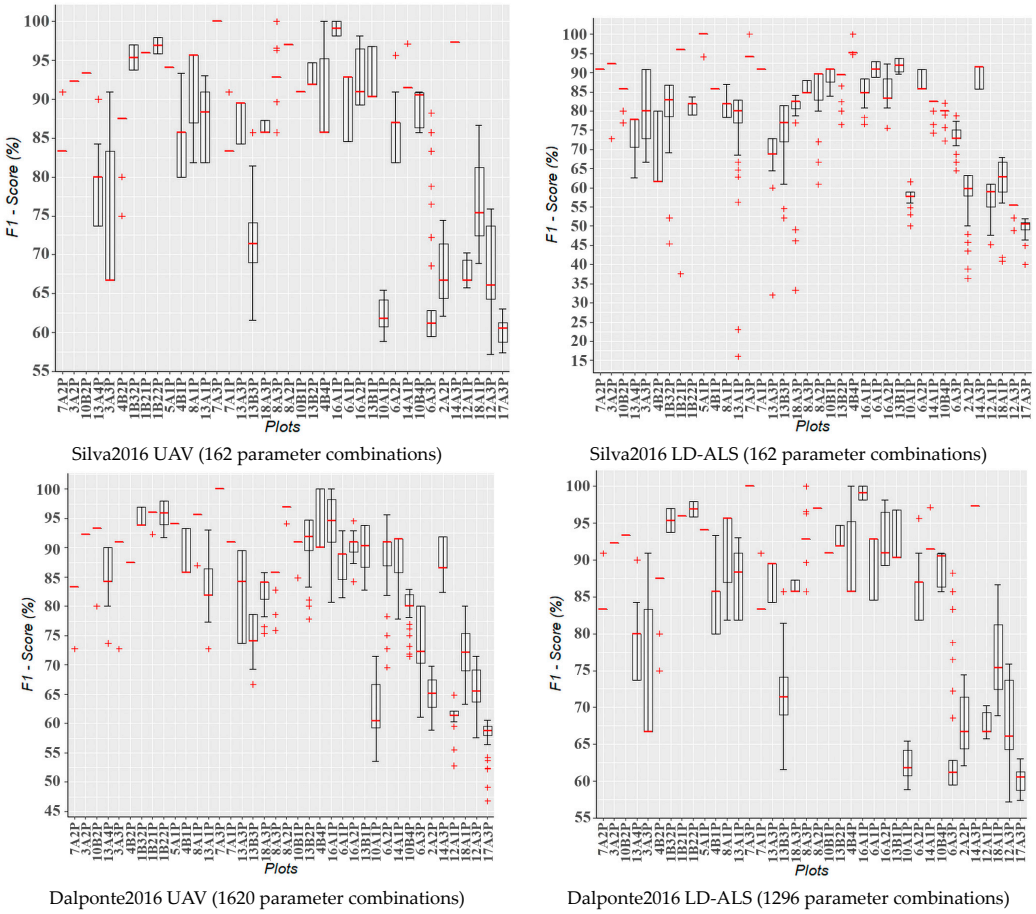


Figure 3. *Cont.*

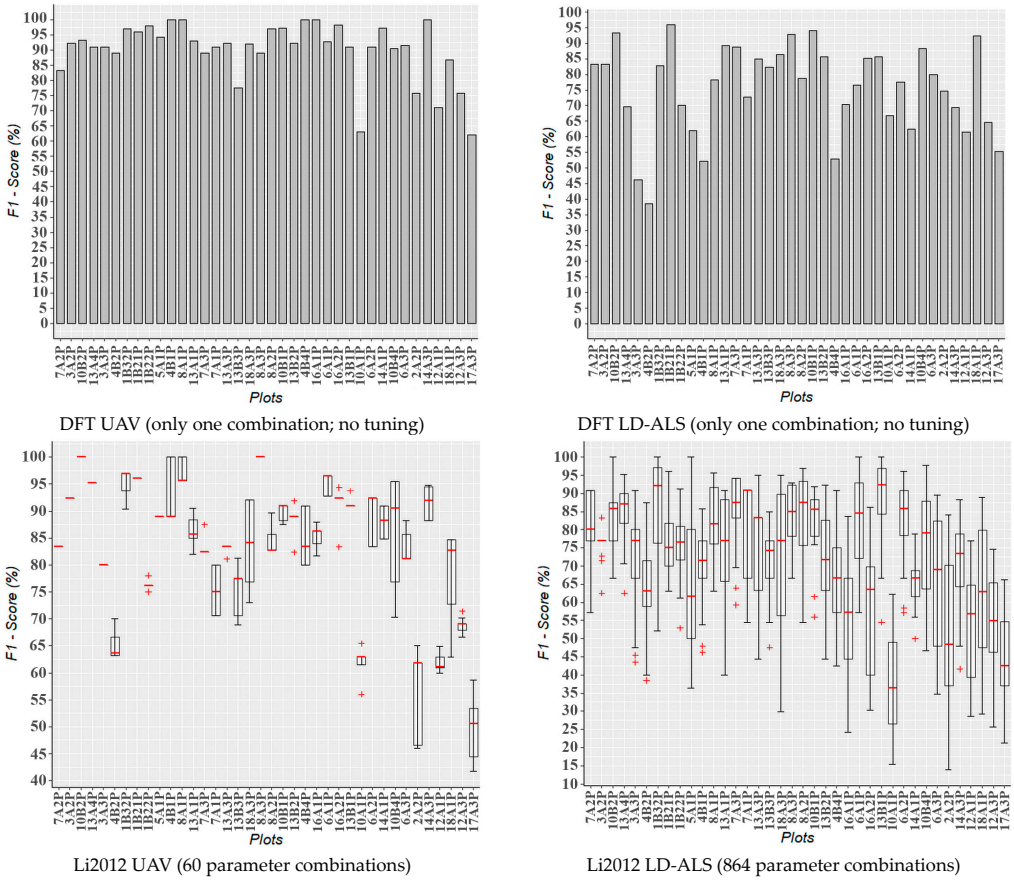


Figure 3. Box-and-whisker plots (histogram in case of DFT method) to estimate the detection accuracy of individual trees in terms of F1-score. The reference plots (X-axis) are arranged in ascending order of vegetation cover. The number of parameter combinations (outputs) is indicated in parentheses. In each box, the center mark indicates the corresponding median value (line in red). Outliers are represented individually by the "+" markers (symbol in red).

Figure 3 shows the F1-score, which also includes variability across parameter combinations (box-and-whisker plots), for the set of matched trees in each reference plot. Overall, and working with UAV and LD-ALS data, increasing vegetation cover had no significant effect on tree detection.

For Silva2016, 162 parameter combinations are represented for both UAV and LD-ALS data (Figure 3). As noted above, the accuracy results were always better when using UAV data. In some reference plots (e.g., reference plot 3A2P in the UAV case and reference plot 7A2P in the LD-ALS case), the median lines and the 25th and 75th percentiles coincided. This means that parameter tuning did not influence the result. These cases are repeated in several plots and for all tested algorithms, especially in plots with low vegetation cover. The rest of the plots showed large boxes, meaning a high dispersion of the F1-score. This dispersion was similar when working with UAV and LD-ALS data, although in the case of LD-ALS there were more dispersed outliers. The median values ranged from 60.55% to 100% and 50.49% to 100% for the UAV and LD-ALS data, respectively.

In the case of Dalponte2016, the boxes represent the results of 1620 parameter combinations for UAV data and 1296 for LD-ALS data. In terms of F1-score, the tree detection results were better when working with high-density UAV data. Even though this region-growing algorithm applies a different strategy compared to the centroidal Voronoi tessellation used by Silva2016, the results turned out to be very similar, except for the observation of more outliers in the case of working with UAV data. Thus, the median values ranged from 58.72% to 100% and 44% to 100% for the UAV and LD-ALS data, respectively.

Regarding the DFT algorithm, it proved to be very effective, especially considering that it does not need to adjust any parameter. The results were reasonably acceptable, providing F1-score values higher than 62.07% and 38.46% for the UAV and LD-ALS data, respectively.

The results yielded by the tested RB algorithms applied to UAV data showed that the lowest value corresponded to the plot with the highest vegetation cover (i.e., plot 17A3P with 86.79% VC). This result may be attributed to issues associated with variation in light reflectance, shadows, occlusion, canopy overlap and closure, and size and tree spacing, as concluded in other similar studies (e.g., [39,76,87,101–103]). Trees located under other trees, trees found in shadows, trees having low spectral contrast with respect to the understory vegetation, or the proximity of trees to neighboring trees are considered determining conditions for the detection of trees [89].

In the case of the LD-ALS data, the Li2012 algorithm proved to be the most effective in most reference plots for the individual tree extraction phase. With 60 parameter combinations for UAV data and 864 for LD-ALS data, this algorithm was demonstrated to be more sensitive to parameter tuning, showing a high dispersion of F1-score values, especially in those reference plots presenting large vegetation cover. In fact, this PCB algorithm was the one that showed the clearest inverse relationship between VC and tree detection accuracy (bottom of Figure 3). In these cases, high rates of under-segmentation were observed due to the significant overlap between nearby trees.

3.3. Accuracy of Tree Height Estimation

Table 6 shows the statistical parameters calculated to assess the accuracy of estimated tree heights such as mean, median, RMSE, relative RMSE, and Pearson´s r.

Table 6. Accuracy of tree height estimation for Silva2016, Dalponte2016, DFT, and Li2012 algorithms given by H mean error (m), H median error (m), H RMSE (m), H relative RMSE (%), and H Pearson´s r, using UAV and LD-ALS data.

Algorithm	CHM	UAV					LD-ALS				
		H Mean Error	H Median Error	H RMSE	H Relative RMSE	H Pearson's r	H Mean Error	H Median Error	H RMSE	H Relative RMSE	H Pearson's r
Silva2016	Best of P2R-MF and PF-MF	0.038	0.01	0.23	2.61	0.97	−0.19	−0.22	0.47	5.44	0.94
	P2R-MF	0.041	0.01	0.23	2.60	0.97	−0.19	−0.22	0.47	5.44	0.94
	PF-MF	0.042	0.01	0.24	2.68	0.97	−0.20	−0.23	0.48	5.54	0.93
Dalponte2016	Best of P2R-MF and PF-MF	0.031	0.01	0.23	2.64	0.98	−0.20	−0.23	0.48	5.45	0.94
	P2R-MF	0.042	0.01	0.22	2.54	0.98	−0.20	−0.23	0.46	5.26	0.95
	PF-MF	0.031	0.01	0.24	2.68	0.97	−0.22	−0.23	0.43	5.12	0.94
DFT	IDW-GF	0.004	−0.01	0.17	2.02	0.99	−0.24	−0.27	0.54	6.09	0.93
Li2012	-	−0.022	0.00	0.39	4.35	0.96	−0.26	−0.23	0.49	6.01	0.94

Although all algorithms attained good results using UAV data, DFT slightly outperformed the other methods, showing a mean error of 0.4 cm. All algorithms provided low systematic errors, especially in the case of the median error, with values less than 2 cm.

In the case of random error, the RMSE yielded values less than 40 cm, leading to a relative RMSE of less than 4.3%. These results were confirmed by analyzing the results of Pearson's r coefficients, with values greater than 0.97. This meant a very good linear fit between the estimated and observed heights. It is worth noting that the order of the algorithms from best to worst was exactly the opposite of that found in the tree detection phase, which is related to the fact that those algorithms that incurred a greater omission error compared fewer trees than others.

The same trend could be observed when segmentation was performed using LD-ALS data. In this case, the Li2012 algorithm obtained the best results in the ITD step, although the results of the H estimation were slightly inferior to those of the other algorithms. Regarding the systematic error, the bias showed values better than −26 cm and −27 cm for the mean and median height error, respectively, which pointed to a significant underestimation of the "real" tree height when working with LD-ALS data. Regarding the random error, the RMSE showed values less than 54 cm, which led to a relative RMSE of less than 6.09%. All

algorithms provided a good fit between the estimated and observed heights, which was reflected in Pearson's linear correlation values greater than 0.93.

3.4. Crown Diameter

Table 7 presents the statistical parameters calculated to assess the accuracy of the estimated crown diameters, such as mean, median, RMSE, relative RMSE, and Pearson's coefficient of linear correlation.

Table 7. Tree crown diameter assessment for Silva2016, Dalponte2016, DFT, and Li2012 algorithms in terms of CD mean error (m), CD median error (m), CD RMSE (m), CD relative RMSE (%), and Pearson's coefficient of linear correlation, using UAV and LD-ALS data.

Algorithm	CHM	UAV					LD-ALS				
		CD Mean Error	CD Median Error	CD RMSE	CD Relative RMSE	CD Pearson's r	CD Mean Error	CD Median Error	CD RMSE	CD Relative RMSE	CD Pearson's r
Silva2016	Best of P2R-MF and PF-MF	−0.52	−0.48	0.92	20.57	0.78	−0.04	−0.05	0.64	15.24	0.75
	P2R-MF	−0.65	−0.62	1.04	23.01	0.78	−0.10	−0.09	0.68	15.92	0.75
	PF-MF	−0.58	−0.55	0.98	21.75	0.73	−0.08	−0.03	0.75	17.91	0.69
Dalponte2016	Best of P2R-MF and PF-MF	−0.18	−0.13	0.74	18.54	0.78	−0.01	−0.02	0.84	19.98	0.65
	P2R-MF	−0.13	−0.09	0.68	16.62	0.79	0.04	0.04	0.80	18.89	0.66
	PF-MF	−0.25	−0.20	0.88	21.17	0.76	−0.33	−0.33	0.88	21.18	0.62
DFT	IDW-GF	0.38	0.32	0.83	19.73	0.84	−0.28	−0.27	1.27	28.81	0.61
Li2012	-	1.91	1.89	2.85	68.34	0.25	1.86	1.89	2.47	56.90	0.57

The results shown in Table 7 correspond to the errors calculated when the best F1-score was obtained, so they should be analyzed taking into account the commission and omission errors in the tree detection phase. In the case of UAV data, and with the exception of the DFT algorithm, all RB algorithms presented a negative systematic error, which implies an underestimation of the crown diameters. In contrast, the DFT and Li2012 algorithms tended to show a positive systematic error, which means an overestimation of the crown diameters. It is necessary to highlight the excessive errors obtained using the Li2012 method, with an average error close to 2 m. The random error (RMSE) took values that ranged between 0.68 m and 2.85 m, with the Li2012 algorithm presenting the worst results. These RMSE values meant a relative RMSE error ranging between 16.62% and 23.01% for the RB algorithms, taking even higher values (68.34%) in the case of the PCB algorithm. The best fit between the estimated and observed CD values, given by the Pearson's linear correlation coefficient, was achieved using the DFT algorithm, obtaining a linear correlation coefficient of 0.84. This fact was also observed at the plot level, as the DFT algorithm stood out with high Pearson's linear correlation coefficient values for the estimated and observed CD values in almost all reference plots.

As for the LD-ALS data, almost all RB algorithms yielded negative systematic errors, indicating an underestimation of the field-measured CDs. Note that these errors were smaller than those obtained using the UAV data. This makes sense given that the algorithms detected more trees working with UAV data compared to the percentage of tree detection working with LD-ALS data. The Li2012 method clearly overestimated the field-measured CDs, showing a very similar result to that obtained using the UAV data. The random error (RMSE) ranged from 0.64 m to 2.47 m, with the Li2012 method obtaining the worst results. The extraction of the crown diameter of individual trees was generally successful using RB algorithms. The Silva2016 algorithm achieved the highest Pearson's coefficient values (r = 0.75), indicating a reasonably good linear correlation between the observed and estimated CD values.

3.5. Combined Accuracy Index

For all algorithms tested in this study, the three best-rewarded CAIs were selected and assigned to three categories (gold, silver, and bronze medals). It is worth noting that medals of the same color have been awarded to versions of the same algorithm (i.e., versions that differ in the way of constructing the CHM) that occupied successive positions in the ranking according to their CAI (see Table 8).

Table 8. Combined accuracy index (CAI) computed for Silva2016, Dalponte2016, DFT, and Li2012 algorithms. The top three algorithms were ranked and grouped into gold, silver, and bronze classes.

Algorithm	CHM	UAV		LD-ALS	
		CAI (%)	Category	CAI (%)	Category
Silva2016	Best of P2R-MF and PF-MF	89.58	Silver	83.83	Silver
	P2R-MF	89.34	Silver	83.54	Silver
	PF-MF	87.95	Silver	81.64	Silver
Dalponte2016	Best of P2R-MF and PF-MF	88.27	Bronze	80.97	Bronze
	P2R-MF	87.87	Bronze	80.82	Bronze
	PF-MF	86.76	Bronze	79.29	Bronze
DFT	IDW-GF	90.46	Gold	76.06	
Li2012	-	79.04		85.31	Gold

Regarding the UAV data and in view of the results, it can be highlighted that the gold medal went to the DFT algorithm based on marker-controlled watershed segmentation. This method yielded the best results, reaching a CAI of 90.46%. The silver medal was awarded to another RB algorithm, Silva2016, which showed slightly lower CAI values than DFT. The bronze medal went to Dalponte2016, the third RB algorithm. Outside the podium, we find Li2012, the only PCB algorithm tested in this study. This algorithm achieved good results both in the tree detection stage and in estimating tree height, but poor results when delineating crown diameters. In addition to the poor CD delineation results, this algorithm turned out to be very slow in processing point cloud data. As described above, Li2012 is not parallelized and has a high algorithmic complexity. Thus, the average processing time, calculated in seconds per million points processed (spm), took a value of 755.79 spm for UAV data and 65.66 spm for LD-ALS data. This processing time included only the segmentation step, without considering input data generation or external preprocessing. All calculations were run with Intel® CoreTM i7-8565U 4 × 1.99 GHz, 16 GB RAM, and NVIDIA Quadro P520.

As for the LD-ALS data, the gold medal clearly went to the Li2012 algorithm, achieving a CAI of 85.31%. This method obtained very good results in the ITD and H estimation phases, although it was ranked the worst in CD estimation. The silver medal was awarded to the Silva2016 algorithm, achieving a CAI value of 83.83% by fitting both the input CHM and the Silva2016 parameters. Similar results were obtained using the CHM generated with the P2R algorithm. The Dalponte2016 algorithm, with CAI values higher than 79%, achieved the bronze medal, while the fourth place went to the DFT algorithm, recording a CAI of 76.06%.

Since one of the objectives of this study was to automate the extraction of trees and their corresponding dendrometric features over large areas, the parameter sets corresponding to each algorithm were analyzed to select the most suitable one to be applied in large-scale mapping. Therefore, the parameter sets that most frequently yielded the best results in terms of CAI were selected. In this way, a second "round" of individual tree segmentation was performed by applying the selected parameter set of each algorithm to all reference plots.

The best results obtained by applying the same set of parameters to all reference plots are detailed in Table 9, while the final selected parameter sets are depicted in Table 10. For the UAV data, the DFT algorithm, with a CAI of 90.46%, ranked first (gold medal). It should be noted again that this algorithm does not need parameter tuning and positively passed the three crucial phases required for the tested algorithms. In fact, it extracted single trees with an F1-score of 90%, also very accurately estimating tree height (H Pearson's r = 0.99) and presenting an acceptable accuracy when extracting crown diameters (CD Pearson's r = 0.84).

Table 9. Tree detection accuracy (F1-score), and tree height and crown diameter assessment (H Pearson´s r, CD Pearson´s r, and combined accuracy index (CAI)) computed for the Silva2016, Dalponte2016, DFT, and Li2012 algorithms applying the same sets of parameters (large-scale mapping) to the 38 reference plots. The three best algorithms have been ranked as gold, silver, and bronze medals.

Algorithm	CHM	UAV				LD-ALS			
		F1-Score	H Pearson's r	CD Pearson's r	CAI (%)	F1-Score	H Pearson's r	CD Pearson's r	CAI (%)
Silva2016	P2R-MF	0.88	0.98	0.70	86.80	0.83	0.94	0.68	82.40
	PF-MF	0.88	0.98	0.70	86.80	0.81	0.94	0.69	81.15
Dalponte2016	P2R-MF	0.87	0.98	0.77	87.15	0.80	0.94	0.25	73.85
	PF-MF	0.86	0.98	0.76	86.30	0.79	0.94	0.20	72.40
DFT	IDW-GF	0.90	0.99	0.84	90.46	0.76	0.93	0.61	76.30
Li2012	-	0.85	0.96	0.21	77.05	0.83	0.94	0.55	80.45

Table 10. Parameter sets corresponding to the best results in terms of CAI applied to the 38 reference plots. (*): see Tables 1–3 for a detailed description of the parameters.

Algorithm	CHM	Parameter (*)	UAV	LD-ALS
Silva2016	P2R-MF	max_cr_factor	0.2	0.3
		exclusion	0.3	0.4
	PF-MF	max_cr_factor	0.2	0.4
		exclusion	0.3	0.5
Dalponte2016	P2R-MF	th_tree	2.00	2.00
		th_seed	0.10	0.20
		th_cr	0.10	0.10
		max_cr	10.00	4.00
	PF-MF	th_tree	2.00	2.00
		th_seed	0.40	0.10
		th_cr	0.50	0.10
		max_cr	10.00	4.00
DFT	IDW-GF	-	-	-
Li2012	-	dt1	1.40	2.00
		dt2	2	2.2
		R	1	2
		Zu	15	15
		hmin	2	2
		Speed-up	5	5

Regarding the LD-ALS data, the same errors were observed. In this case, the Li2012 algorithm also obtained good results both in tree segmentation and height extraction. As can be seen in Table 9, Li2012 achieved an F1-score value of 0.83 and an H Pearson's r of 0.94. These results were identical to those provided by the Silva2016 algorithm that obtained the gold medal in this second round. However, the CD delineation results were not good, showing a low Pearson's r of 0.55. For its part, Silva2016 managed to yield good results in terms of CD extraction, which allowed it to rise to the first position in the ranking with fairly good CAI values of 82.40% and 81.15% using P2R and PF, respectively. In this sense, Silva2016 can be qualified as the best choice for performing large-scale mapping from LD-ALS data in Mediterranean forests. On the other hand, the DFT algorithm achieved the bronze medal, showing a CAI of 76.30%, while Dalponte2016 was left out of the podium. In this case, it can be observed that the quality of CD delineation was significantly reduced when the same set of parameters was applied to all reference plots. This fact was reflected in some really bad Pearson's r values.

4. Discussion

In this study, a comprehensive comparative analysis was carried out including four different ITD approaches to detect trees and extract their height and crown diameter based on point clouds from UAV images and low-density airborne laser scanning. Furthermore, the importance of the preprocessing stage in building the CHM in raster-based approaches was also investigated, exploring the multifactorial effect on the final accuracy of various parameter combinations for each algorithm, preprocessing factors, and point cloud types. After finding the best combination of factors for each reference plot, the optimal combination of parameters to obtain the best results from UAV and LD-ALS point clouds is also provided, which can be applied to perform automated inventories of Mediterranean forests (Aleppo pine). It is noteworthy that, unlike previous studies, our goal is to select the best parameters for each tested algorithm and point cloud type to extract as accurately as possible tree locations, tree heights, and crown diameters over a wide geographic area (large-scale mapping). These dendrometric features can be used to obtain estimates of AGB and stem volume, thus helping to develop effective national REDD (Reducing Emissions from Deforestation and Forest Degradation) programs and sustainable forest management.

As we will discuss later, it is especially relevant to be able to obtain reasonably accurate results using low-density ALS data, thus taking advantage of ALS data that are usually available at a national scale in several countries (e.g., PNOA: National Plan for Aerial Orthophotography of Spain).

Below, we will discuss the results obtained in each of the phases into which the study can be divided: detection of individual trees, estimation of tree height, estimation of crown diameter, and, finally, large-scale mapping using the combined accuracy index to select the optimal combination of parameters.

4.1. Individual Tree Detection

It should be noted that, despite the diversity of applied approaches, ITD results had similar accuracy. Regarding point clouds derived from UAV-SfM photogrammetry, and after an exhaustive tuning of the input parameters (CHM construction and parameter sets of each segmentation algorithm), it could be concluded that the local maxima algorithm (variable window size) together with the raster-based algorithm based on the calculation of a centroidal Voronoi tessellation (Silva2016) obtained better results (F1-score = 90.47%). Zaforemska et al. [49] and Torresan et al. [52] reported that a certain degree of parameter tuning procedure is necessary to optimize the segmentation process and to obtain the best results. In any case, the Silva2016 algorithm proved to be also a good choice for performing large-scale forest mapping after finding its optimal combination of parameters for the study area, yielding an F1-score > 0.88.

Marker-controlled watershed segmentation, within the pipeline of the DFT method in this study [85], also provided good results when dealing with UAV point clouds. This algorithm turned out to be a good choice for working on large-scale forest mapping, especially considering that it does not require parameter tuning and that it is fast compared to the PCB algorithm. It should be noted that for the LM extraction, we used the approach proposed by Popescu and Wynne [90] to relate the size of the search window for extracting local maxima and the height of the tree (see Equation (1)). This general relationship was developed for conifer stands with settings typical of the southeastern United States. Although this model worked reasonably well in our case, the results could be even better if allometric equations with local calibration between tree height and crown width were available. Working with an LM algorithm and a CHM derived from UAV-SfM products, Mohan et al. [104] achieved similar accuracy (F1-score > 0.80) for ITD. In this work, the authors suggest that the right combination of the LM algorithm, a suitable tree window size, and an adequate smoothing window size may be a good choice for the ITD task. Belmonte et al. [105], working in a ponderosa pine forest located at the base of the San Francisco Peaks, reported that the F1-score ranged from approximately 0.44 to 0.94, depending on the tree density. In the same sense, Young et al. [67] obtained F1-score values ranging between

0.67 and 0.83, when considering all the trees, and between 0.78 and 0.87, when classifying only the dominant trees. Other authors obtained similar results, with F1-scores ranging from 0.6 to 0.77 [97,106].

As a relevant note, the PCB algorithm published by Li et al. [94] achieved the best results working with LD-ALS data point clouds, which is in line with other studies. For example, Hauglin and Næsset [107] tested four algorithms (three RB and one PCB) for ITD using ALS data (8 points/m^2). The results highlighted that the PCB algorithm performed best in plots with low tree density, but was worse as tree density increased. Using high-resolution UAV-Lidar data and adopting the Li2012 approach, Wallace et al. [27] were able to correctly segment 91% of the trees in six circular plots of a Tasmanian blue gum plantation. Kaartinen et al. [47] obtained ITD values ranging from 25% to 102% using ALS data with point densities of 2, 4, and 8 points/m^2. In this latter study, it could be highlighted that the point density had a minor impact on the segmentation rate and that taller trees were detected with greater accuracy.

4.2. Tree Height Estimation

All algorithms performed well in extracting tree heights. The RB algorithms performed well in estimating height, with a mean error of H ranging from 0.4 cm to 4.2 cm when using the 3D UAV photogrammetry data. Looking at the height estimation bias, it can be seen that all RB algorithms applied to the UAV data have slightly overestimated tree height values. This finding points to either (i) a very slight underestimation of tall tree heights during ground surveys, or (ii) a very slight overestimation of tree heights by the photogrammetry matching algorithm. In any case, the bias can be considered practically negligible in the case of high-density point clouds derived from UAV data.

The results were also good when working with LD-ALS data. In this case, the mean error of H was better than −26 cm for all tested algorithms, with a clear underestimation of tree height in all cases. This underestimation has been reported in other studies (e.g., [64,83,108]), being explained by the low ALS data density and the subsequent low probability of the laser pulses hitting the tree apex. Another plausible explanation for this fact may be the partial penetration of the Lidar signal inside the cover before the Lidar receiver can detect a return [109]. Note that the two different remote sensing methods used in this study to generate the baseline data to extract the forest inventory are very different and do not observe forest structure the same way. Lidar uses active systems and emits pulses of light that penetrate the vegetation profile, usually providing ground reference. Three-dimensional UAV photogrammetry point clouds are generated through dense feature matching across multiple images, while ground control points (GCPs) are used for georeferencing and scaling steps [110]. These data represent only the top or envelope component of tree canopies and only provide a ground reference when tree density allows. In fact, the use of UAV-based data and SfM algorithms to compute CHMs in dense forests is somewhat limited due to their inefficiency in generating accurate DTMs independently [69]. These limitations can directly influence the height extraction results. The good results obtained in this study indicate that the pipeline adopted for the preparation of the input data was technically sound.

4.3. Crown Diameter Estimation

Crown diameter extraction was generally more successful using raster-based algorithms for both UAV and LD-ALS data, showing a maximum mean error of 65 cm. Previous studies reported that these methods based on raster CHM construction are typically more efficient, although some information is inevitably lost when 3D point clouds are converted to 2D rasters [76]. The only point cloud-based algorithm tested in this study clearly overestimated the CDs measured in the field, showing mean errors close to 2 m. Torresan et al. [52] reported that the Li2012 algorithm showed a clear tendency to group crowns of more than one tree in a mountainous area in Italy. As a result, it tended to delineate larger crowns than existed in reality (under-segmentation error). In terms of tree crown delineation,

the point cloud-based algorithms decompose directly the point cloud data into different homogenous groups [111]. Xu et al. [112] reported that the performance of this kind of algorithm is affected by (i) unevenly distributed point clouds, (ii) localized data deficiency caused by occlusion, and (iii) pendulous branches that yield certain conjunctions with neighboring crowns.

The four algorithms tested in this study provide different and interesting solutions for determining crown diameters in Mediterranean forests, but they pose some problems that need to be solved. In fact, and in view of the results discussed above, the most challenging and critical phase for all the algorithms tested and data types (UAV and LD-ALS) consisted of extracting the diameters of the crowns. Working in the same study area, Aguilar et al. [8] demonstrated that DBH can be predicted with acceptable accuracy using only tree height. However, multivariate allometric models to predict DBH provided much better results, both in terms of goodness-of-fit and stability of the regression models, when both H and CD were included as predictor variables.

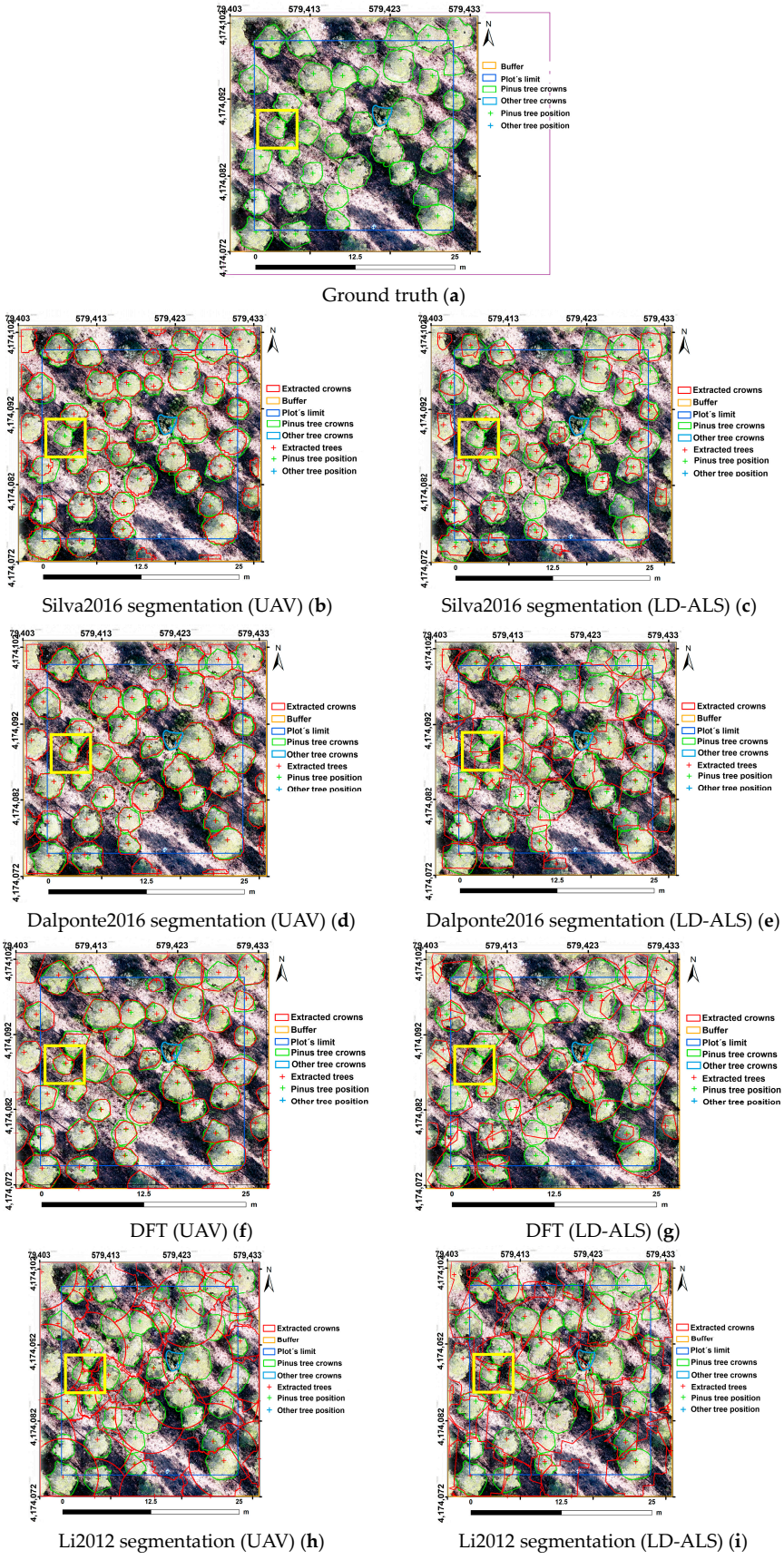
4.4. ITD, H, and CD Extraction (Combined Accuracy Index)

The DFT method applied to raster point clouds obtained by UAV showed a high F1-score of 90.02%, also achieving good scores in the estimation of tree height (Pearson's r = 0.99) and crown diameter (Pearson's r = 0.84). These good results implied a combined accuracy index that reached values above 90%. This algorithm proved to be a good choice for working on large-scale forest mapping, especially considering that it does not require parameter tuning. The other RB algorithms tested in this work yielded slightly lower CAI values (CAI > 86%).

As for the LD-ALS point clouds, it is an important finding to highlight that they have also proven to be a good option to accurately extract individual trees and their corresponding crown heights and diameters. This finding is especially relevant if we consider the growing availability of ALS data programs at a national scale, such as the National Plan for Aerial Orthophotography (PNOA), which represents a great opportunity to have updated and freely accessible ALS data for large-scale forest mapping. After applying an appropriate parameter setting for each reference plot, the Li2012 algorithm showed the best results, reaching a CAI of 85.31%. It gave very good results both in the ITD stage (F1-score > 89%) and in the H estimation (relative RMSE of 6.01% and Pearson's r of 0.94), but failed in CD extraction (relative RMSE of 56.90% and Pearson's r of 0.57).

By applying the same set of parameters to all reference plots (large-scale mapping), the centroidal Voronoi tessellation algorithm emerged as the best, although closely followed by the Li2012 algorithm. In this case, 0.3 and 0.4 were the optimal thresholds for the max_crown and the exclusion parameters, respectively, while the P2R method would be recommended to build the input CHM. Note that Silva2016 uses an LM method based on a circular variable tree window size to detect treetops. By setting these parameters, it was possible to achieve the best results, with a final CAI of 82.40% (F1-score = 0.83, H Pearson´s r = 0.94, CD Pearson´s r = 0.68).

These results can be clearly seen in Figure 4, which shows the segmentation results of all the tested algorithms in the case of the reference plot 16A1P. It is worth mentioning that the DFT (marker-controlled watershed) was the only one able to extract 100% of the trees in this AoI. This figure shows the case of the tree, marked with the yellow square, that no other algorithm was able to segment correctly. Furthermore, the effect of limiting the minimum tree height to 2 m can be seen both in the LM function and in the segmentation algorithms. Thanks to this option, no trees below this height were included in the tree detection process. This is the case for the trees outlined in cyan (see Figure 4). The silver medal went to the Dalponte2016 algorithm applied to the input CHM generated by the P2R algorithm. Very closely, the Silva2016 algorithm, working with the PF-CHM and the P2R-CHM input options, took the third position. The Li2012 algorithm ranked last. Despite achieving good results for tree segmentation and tree height estimation, it failed to determine the crown diameter. This can be clearly seen in Figure 4h, where the algorithm makes many errors.



Ground truth (**a**)

Silva2016 segmentation (UAV) (**b**)

Silva2016 segmentation (LD-ALS) (**c**)

Dalponte2016 segmentation (UAV) (**d**)

Dalponte2016 segmentation (LD-ALS) (**e**)

DFT (UAV) (**f**)

DFT (LD-ALS) (**g**)

Li2012 segmentation (UAV) (**h**)

Li2012 segmentation (LD-ALS) (**i**)

Figure 4. Ground truth (in green) and tree segmentation results after applying the same sets of parameters (in red) to the reference plot 16A1P. Trees with heights less than 2 m are delineated in cyan

("other trees" in the legend). (**a**) Ground truth. (**b**) Silva2016 applied to UAV data using PF-CHM. (**c**) Silva2016 applied to LD-ALS data using PF-CHM. (**d**) Dalponte2016 applied to UAV data using P2R-CHM. (**e**) Dalponte2016 applied to LD-ALS data using P2R-CHM. (**f**) DFT applied to UAV data. (**g**) DFT applied to LD-ALS data. (**h**) Li2012 applied to UAV data. (**i**) Li2012 applied to LD-ALS data.

Finally, it is worth highlighting that the state-of-the-art approaches use the forest variables automatically estimated in this study to make spatiotemporal predictions of aboveground biomass (AGB) over large-scale areas. An example of these functions is the agb function included in the itcpackage R [113]. This function implements the allometric equation proposed in [114]. In our particular study area, the AGB could be calculated using the Aleppo pine allometric equations reported in [8]. Trees with a DBH less than 7.5 cm and a height less than 2 m, in addition to the biomass of the shrub fraction, could be estimated using the method proposed by [115] according to the categories established in [116]. This task related to large-scale AGB mapping will be part of further works carried out by the authors of this publication.

5. Conclusions

This paper comprehensively compared the performance of ITD in Mediterranean forest based on point clouds from UAV and LD-ALS data. Four different algorithms, three RB and one PCB, were tested. The obtained results demonstrated that the pipeline proposed in this work could be used to accurately extract individual trees (tree location) and some of their dendrometric parameters, such as tree height and crown diameter, in the context of Mediterranean coniferous forests.

After intensive experiments, consisting of tuning the input parameters, it could be concluded that the combination of the local maxima with variable window size and marker-controlled watershed segmentation (DFT approach) provided better results when dealing with UAV-derived point clouds. On the other hand, the Li2012 approach provided the best results when working with low-density ALS point clouds.

The DFT approach applied to the CHM constructed from UAV point clouds showed a high F1-score of 90.02%, also achieving good scores in estimating tree height (Pearson's r = 0.99) and crown diameter (Pearson's r = 0.84). This method proved to be a good choice to work on large-scale forest mapping, especially considering that it does not require parameter tuning. When this method was applied to all reference plots using the same set of parameters (large-scale mapping), the combined accuracy index introduced in this study showed good results, reaching a value of 90.46%.

As for the LD-ALS point clouds, it is important to highlight that they have also proven to be a good option to accurately extract individual trees and their corresponding crown heights and diameters. After applying a suitable parameter setting for each reference plot, the Li2012 algorithm showed the best results, reaching a CAI of 85.31%. However, when applying the same set of parameters to all reference plots, the Silva2016 approach emerged as the best, although closely followed by the Li2012 algorithm. By setting the right parameters, it was possible to achieve the best results, with final CAI values of 82.40% and 80.45% by Silva2016 and Li2012, respectively.

The results obtained in this work would allow for large-scale mapping of Aleppo pine forests in the Sierra de María-Los Vélez Natural Park. Furthermore, and on a practical level, the reader can find in this work the set of recommended parameters for each algorithm tested for both UAV and LD-ALS data. These results can help end users with the application of the different approaches tested in this study and highlight future improvements of the approaches to obtain good results in the large-scale mapping of Mediterranean coniferous forests.

Author Contributions: A.N., F.J.A. and M.A.A. conceived, designed, and performed the experiments; collected and analyzed the data; prepared the figures and tables; and wrote the manuscript draft. All authors have read and agreed to the published version of the manuscript.

Funding: This study was funded by the following research projects: (1) "Enabling interdisciplinary collaboration to foster Mediterranean forest sustainable management and socio-economic valuation (ECO2-FOREST)" (Proyecto Retos Junta de Andalucía, Spain. Grant number P18-RT-2327). (2) "Intervention strategies for an integrated and sustainable management of the Mediterranean forest based on an interdisciplinary analysis and its economic assessment" (Programa Operativo FEDER Andalucía 2014-2020, Spain. Grant number UAL2020-SEJ-D1931).

Data Availability Statement: The data presented in this study are openly available in zenodo at 10.5281/zenodo.10518411.

Acknowledgments: This research was funded by the project ECO2-FOREST (Proyecto Retos Junta de Andalucía, Spain, grant number P18-RT-2327). This work takes part in the general research lines promoted by the Agrifood Campus of International Excellence ceiA3, Spain (http://www.ceia3.es/, accessed on 1 January 2024). We also thank the journal's anonymous reviewers for their valuable comments, which greatly improved the original manuscript.

Conflicts of Interest: The authors declare no conflicts of interest.

References

1. Pan, Y.; Birdsey, R.A.; Fang, J.; Houghton, R.; Kauppi, P.E.; Kurz, W.A.; Phillips, O.L.; Shvidenko, A.; Lewis, S.L.; Canadell, J.G.; et al. A large and persistent carbon sink in the world's forests. *Science* **2011**, *333*, 988–993. [CrossRef] [PubMed]
2. Lal, R. Sequestration of atmospheric CO_2 in global carbon pools. *Energy Environ. Sci.* **2008**, *1*, 86–100. [CrossRef]
3. Tang, L.; Shao, G. Drone remote sensing for forestry research and practices. *J. For. Res.* **2015**, *26*, 791–797. [CrossRef]
4. Mokro, M.; Liang, X.; Surový, P.; Valent, P.; Čerňava, J.; Chudý, F.; Tunák, D.; Saloň, I.; Merganič, J. Evaluation of Close-Range Photogrammetry Image Collection Methods for Estimating Tree Diameters. *ISPRS Int. J. Geo-Inf.* **2018**, *7*, 93. [CrossRef]
5. Peñalver Romeo, A.; Aguilar Torres, F.J.; Nemmaoui, A.; Rivas Barzola, J.R.; Triana Tomalá, Á.A.; Aguilar Torres, M.A.; Llanderal, A. Precisión y eficiencia del inventario de plantaciones de teca en Ecuador mediante escáner láser terrestre. *Madera Y Bosques* **2021**, *27*, e2712097. [CrossRef]
6. Avery, T.; Burkhart, H.E. *Forest Measurements*, 4th ed.; McGraw-Hill, Inc.: Boston, MA, USA, 1994; ISBN 0070025568.
7. Kwak, D.A.; Lee, W.K.; Lee, J.H.; Biging, G.S.; Gong, P. Detection of individual trees and estimation of tree height using LiDAR data. *J. For. Res.* **2007**, *12*, 425–434. [CrossRef]
8. Aguilar, F.J.; Nemmaoui, A.; Aguilar, M.A.; Jiménez-Lao, R. Aleppe Pine Allometric Modeling Through Integrating UAV Image-Based Clouds and Ground Based Data. *ISPRS Ann. Photogramm. Remote Sens. Spat. Inf. Sci.* **2022**, *3*, 353–360. [CrossRef]
9. Atzberger, C.; Zeug, G.; Defourny, P.; Aragão, L.; Hammarström, L.; Immitzer, M. *Monitoring of Forests Through Remote Sensing—Final Report*; EU Commission: Luxembourg, 2020.
10. Lamping, J.E.; Zald, H.S.J.; Madurapperuma, B.D.; Graham, J. Comparison of Low-Cost Commercial Unpiloted Digital Aerial Photogrammetry to Airborne Laser Scanning across Multiple Forest Types in California, USA. *Remote Sens.* **2021**, *13*, 4292. [CrossRef]
11. Jayathunga, S.; Owari, T.; Tsuyuki, S. The use of fixed–wing UAV photogrammetry with LiDAR DTM to estimate merchantable volume and carbon stock in living biomass over a mixed conifer—Broadleaf forest. *Int. J. Appl. Earth Obs. Geoinf.* **2018**, *73*, 767–777. [CrossRef]
12. Eysn, L.; Hollaus, M.; Lindberg, E.; Berger, F.; Monnet, J.-M.; Dalponte, M.; Kobal, M.; Pellegrini, M.; Lingua, E.; Mongus, D.; et al. A Benchmark of Lidar-Based Single Tree Detection Methods Using Heterogeneous Forest Data from the Alpine Space. *Forests* **2015**, *6*, 1721–1747. [CrossRef]
13. Lefsky, M.A.; Cohen, W.B.; Parker, G.G.; Harding, D.J. Lidar Remote Sensing for Ecosystem StudiesLidar, an emerging remote sensing technology that directly measures the three-dimensional distribution of plant canopies, can accurately estimate vegetation structural attributes and should be of particular intere. *Bioscience* **2002**, *52*, 19–30. [CrossRef]
14. Appiah Mensah, A.; Jonzén, J.; Nyström, K.; Wallerman, J.; Nilsson, M. Mapping site index in coniferous forests using bi-temporal airborne laser scanning data and field data from the Swedish national forest inventory. *For. Ecol. Manag.* **2023**, *547*, 121395. [CrossRef]
15. Vosselman, G.; Maas, H.-G. *Airborne and Terrestrial Laser Scanning*; Whittles Publishing: Dunbeath, UK, 2010; ISBN 978-1-904445-87-6.
16. Hodgson, M.E.; Bresnahan, P. Accuracy of airborne lidar-derived elevation: Empirical assessment and error budget. *Photogramm. Eng. Remote Sens.* **2004**, *70*, 331–339. [CrossRef]
17. Fernández-Guisuraga, J.M.; Suárez-Seoane, S.; Fernandes, P.M.; Fernández-García, V.; Fernández-Manso, A.; Quintano, C.; Calvo, L. Pre-fire aboveground biomass, estimated from LiDAR, spectral and field inventory data, as a major driver of burn severity in maritime pine (*Pinus pinaster*) ecosystems. *For. Ecosyst.* **2022**, *9*, 100022. [CrossRef]
18. Fernández-Guisuraga, J.M.; Suárez-Seoane, S.; García-Llamas, P.; Calvo, L. Vegetation structure parameters determine high burn severity likelihood in different ecosystem types: A case study in a burned Mediterranean landscape. *J. Environ. Manag.* **2021**, *288*, 112462. [CrossRef]

19. García, M.; Riaño, D.; Chuvieco, E.; Salas, J.; Danson, F.M. Multispectral and LiDAR data fusion for fuel type mapping using Support Vector Machine and decision rules. *Remote Sens. Environ.* **2011**, *115*, 1369–1379. [CrossRef]
20. Gelabert, P.J.; Montealegre, A.L.; Lamelas, M.T.; Domingo, D. Forest structural diversity characterization in Mediterranean landscapes affected by fires using Airborne Laser Scanning data. *GISci. Remote Sens.* **2020**, *57*, 497–509. [CrossRef]
21. Aguilar, F.J.; Nemmaoui, A.; Aguilar, M.A.; Peñalver, A. Building Tree Allometry Relationships Based on TLS Point Clouds and Machine Learning Regression. *Appl. Sci.* **2021**, *11*, 10139. [CrossRef]
22. Aguilar, F.J.; Nemmaoui, A.; Peñalver, A.; Rivas, J.R.; Aguilar, M.A. Developing Allometric Equations for Teak Plantations Located in the Coastal Region of Ecuador from Terrestrial Laser Scanning Data. *Forests* **2019**, *10*, 1050. [CrossRef]
23. Aguilar, F.J.; Nemmaoui, A.; Aguilar, M.A.; Peñalver, A. Fusion of Terrestrial Laser Scanning and RPAS Image Based point cloud in Mediterranean forest inventories. *Dyna Ing. E Ind.* **2019**, *94*, 131–136. [CrossRef]
24. Aguilar, F.J.; Rivas, J.R.; Nemmaoui, A.; Peñalver, A.; Aguilar, M.A. UAV-Based Digital Terrain Model Generation under Leaf-Off Conditions to Support Teak Plantations Inventories in Tropical Dry Forests. A Case of the Coastal Region of Ecuador. *Sensors* **2019**, *19*, 1934. [CrossRef] [PubMed]
25. Liu, Z.; Chen, C.; Huang, Z.; Chang, Y.C.; Liu, L.; Pei, Q. A Low-Cost and Lightweight Real-Time Object-Detection Method Based on UAV Remote Sensing in Transportation Systems. *Remote Sens.* **2024**, *16*, 3712. [CrossRef]
26. Maltamo, M.; Næsset, E.; Vauhkonen, J. *Forestry Applications of Airborne Laser Scanningg: Concepts and Case Studies*; Maltamo, M., Naesset, E., Vauhkonen, J., Eds.; Managing Forest Ecosystems; Springer: Dordrecht, The Netherlands, 2014; Volume 27, ISBN 978-94-024-0611-5.
27. Wallace, L.; Lucieer, A.; Watson, C.S. Evaluating tree detection and segmentation routines on very high resolution UAV LiDAR ata. *IEEE Trans. Geosci. Remote Sens.* **2014**, *52*, 7619–7628. [CrossRef]
28. Wallace, L.; Lucieer, A.; Malenovský, Z.; Turner, D.; Vopěnka, P.; Wallace, L.; Lucieer, A.; Malenovský, Z.; Turner, D.; Vopěnka, P. Assessment of Forest Structure Using Two UAV Techniques: A Comparison of Airborne Laser Scanning and Structure from Motion (SfM) Point Clouds. *Forests* **2016**, *7*, 62. [CrossRef]
29. Paneque-Gálvez, J.; McCall, M.K.; Napoletano, B.M.; Wich, S.A.; Koh, L.P. Small Drones for Community-Based Forest Monitoring: An Assessment of Their Feasibility and Potential in Tropical Areas. *Forests* **2014**, *5*, 1481–1507. [CrossRef]
30. Koh, L.P.; Wich, S.A. Dawn of drone ecology: Low-cost autonomous aerial vehicles for conservation. *Trop. Conserv. Sci.* **2012**, *5*, 121–132. [CrossRef]
31. Lim, Y.S.; La, P.H.; Park, J.S.; Lee, M.H.; Pyeon, M.W.; Kim, J.I. Calculation of Tree Height and Canopy Crown from Drone Images Using Segmentation. *J. Korean Soc. Surv. Geod. Photogramm. Cartogr.* **2015**, *33*, 605–614. [CrossRef]
32. Zarco-Tejada, P.J.; Diaz-Varela, R.; Angileri, V.; Loudjani, P. Tree height quantification using very high resolution imagery acquired from an unmanned aerial vehicle (UAV) and automatic 3D photo-reconstruction methods. *Eur. J. Agron.* **2014**, *55*, 89–99. [CrossRef]
33. Koch, B.; Heyder, U.; Welnacker, H. Detection of individual tree crowns in airborne lidar data. *Photogramm. Eng. Remote Sens.* **2006**, *72*, 357–363. [CrossRef]
34. Koch, B.; Kattenborn, T.; Straub, C.; Vauhkonen, J. Segmentation of Forest to Tree Objects BT—Forestry Applications of Airborne Laser Scanning: Concepts and Case Studies. In *Forestry Applications of Airborne Laser Scanning. Managing Forest Ecosystems*; Maltamo, M., Næsset, E., Vauhkonen, J., Eds.; Springer: Dordrecht, The Netherlands, 2013; pp. 89–112, ISBN 978-94-017-8663-8.
35. Popescu, S.C.; Wynne, R.H.; Nelson, R.F. Measuring individual tree crown diameter with lidar and assessing its influence on estimating forest volume and biomass. *Can. J. Remote Sens.* **2003**, *29*, 564–577. [CrossRef]
36. Hyyppä, J.; Kelle, O.; Lehikoinen, M.; Inkinen, M. A segmentation-based method to retrieve stem volume estimates from 3-D tree height models produced by laser scanners. *IEEE Trans. Geosci. Remote Sens.* **2001**, *39*, 969–975. [CrossRef]
37. Chen, Q.; Baldocchi, D.; Gong, P.; Kelly, M. Isolating individual trees in a savanna woodland using small footprint lidar data. *Photogramm. Eng. Remote Sens.* **2006**, *72*, 923–932. [CrossRef]
38. Jing, L.; Hu, B.; Noland, T.; Li, J. An individual tree crown delineation method based on multi-scale segmentation of imagery. *ISPRS J. Photogramm. Remote Sens.* **2012**, *70*, 88–98. [CrossRef]
39. Silva, C.A.; Hudak, A.T.; Vierling, L.A.; Loudermilk, E.L.; O'Brien, J.J.; Hiers, J.K.; Jack, S.B.; Gonzalez-Benecke, C.; Lee, H.; Falkowski, M.J.; et al. Imputation of individual longleaf pine (*Pinus palustris* Mill.) tree attributes from field and LiDAR data. *Can. J. Remote Sens.* **2016**, *42*, 554–573. [CrossRef]
40. Jakubowski, M.K.; Li, W.; Guo, Q.; Kelly, M.; Jakubowski, M.K.; Li, W.; Guo, Q.; Kelly, M. Delineating Individual Trees from Lidar Data: A Comparison of Vector- and Raster-based Segmentation Approaches. *Remote Sens.* **2013**, *5*, 4163–4186. [CrossRef]
41. Reitberger, J.; Schnörr, C.; Krzystek, P.; Stilla, U. 3D segmentation of single trees exploiting full waveform LIDAR data. *ISPRS J. Photogramm. Remote Sens.* **2009**, *64*, 561–574. [CrossRef]
42. Duncanson, L.I.; Cook, B.D.; Hurtt, G.C.; Dubayah, R.O. An efficient, multi-layered crown delineation algorithm for mapping individual tree structure across multiple ecosystems. *Remote Sens. Environ.* **2014**, *154*, 378–386. [CrossRef]
43. Heinzel, J.N.; Weinacker, H.; Koch, B. Prior-knowledge-based single-tree extraction. *Int. J. Remote Sens.* **2011**, *32*, 4999–5020. [CrossRef]
44. Sačkov, I.; Hlásny, T.; Bucha, T.; Juriš, M. Integration of tree allometry rules to treetops detection and tree crowns delineation using airborne lidar data. *iForest-Biogeosci. For.* **2017**, *10*, 459. [CrossRef]

45. Xu, X.; Iuricich, F.; De Floriani, L. A Persistence-Based Approach for Individual Tree Mapping. In Proceedings of the 28th International Conference on Advances in Geographic Information Systems, Seattle, WA, USA, 3–6 November 2020; pp. 191–194. [CrossRef]
46. Kaartinen, H.; Hyyppä, J. *EuroSDR/ISPRS Project Commission II, Tree Extraction, Final Report*; EuroSDR: Dublin, Ireland, 2008.
47. Kaartinen, H.; Hyyppä, J.; Yu, X.; Vastaranta, M.; Hyyppä, H.; Kukko, A.; Holopainen, M.; Heipke, C.; Hirschmugl, M.; Morsdorf, F.; et al. An International Comparison of Individual Tree Detection and Extraction Using Airborne Laser Scanning. *Remote Sens.* **2012**, *4*, 950–974. [CrossRef]
48. Vauhkonen, J.; Ene, L.; Gupta, S.; Heinzel, J.; Holmgren, J.; Pitkänen, J.; Solberg, S.; Wang, Y.; Weinacker, H.; Hauglin, K.M.; et al. Comparative testing of single-tree detection algorithms under different types of forest. *Forestry* **2012**, *85*, 27–40. [CrossRef]
49. Zaforemska, A.; Xiao, W.; Gaulton, R. Individual Tree Detection from UAV LiDAR Data in a Mixed Species Woodland. *Int. Arch. Photogramm. Remote Sens. Spat. Inf. Sci.* **2019**, *XLII-2-W13*, 657–663. [CrossRef]
50. Edson, C.; Wing, M.G. Airborne Light Detection and Ranging (LiDAR) for Individual Tree Stem Location, Height, and Biomass Measurements. *Remote Sens.* **2011**, *3*, 2494–2528. [CrossRef]
51. Wang, Y.; Hyyppa, J.; Liang, X.; Kaartinen, H.; Yu, X.; Lindberg, E.; Holmgren, J.; Qin, Y.; Mallet, C.; Ferraz, A.; et al. International Benchmarking of the Individual Tree Detection Methods for Modeling 3-D Canopy Structure for Silviculture and Forest Ecology Using Airborne Laser Scanning. *IEEE Trans. Geosci. Remote Sens.* **2016**, *54*, 5011–5027. [CrossRef]
52. Torresan, C.; Carotenuto, F.; Chiavetta, U.; Miglietta, F.; Zaldei, A.; Gioli, B. Individual Tree Crown Segmentation in Two-Layered Dense Mixed Forests from UAV LiDAR Data. *Drones* **2020**, *4*, 10. [CrossRef]
53. Domingo, D.; Lamelas-Gracia, M.T.; Montealegre-Gracia, A.L.; de la Riva-Fernández, J. Comparison of regression models to estimate biomass losses and CO_2 emissions using low-density airborne laser scanning data in a burnt Aleppo pine forest. *Eur. J. Remote Sens.* **2017**, *50*, 384–396. [CrossRef]
54. García-Gutiérrez, J.; Martínez-Álvarez, F.; Troncoso, A.; Riquelme, J.C. A comparison of machine learning regression techniques for LiDAR-derived estimation of forest variables. *Neurocomputing* **2015**, *167*, 24–31. [CrossRef]
55. Shendryk, I.; Hellström, M.; Klemedtsson, L.; Kljun, N. Low-Density LiDAR and Optical Imagery for Biomass Estimation over Boreal Forest in Sweden. *Forests* **2014**, *5*, 992–1010. [CrossRef]
56. Domingo, D.; Alonso, R.; Lamelas, M.T.; Montealegre, A.L.; Rodríguez, F.; de la Riva, J. Temporal Transferability of Pine Forest Attributes Modeling Using Low-Density Airborne Laser Scanning Data. *Remote Sens.* **2019**, *11*, 261. [CrossRef]
57. Viedma, O.; Almeida, D.R.A.; Moreno, J.M. Postfire Tree Structure from High-Resolution LiDAR and RBR Sentinel 2A Fire Severity Metrics in a *Pinus halepensis*-Dominated Burned Stand. *Remote Sens.* **2020**, *12*, 3554. [CrossRef]
58. Guerra-Hernández, J.; Tomé, M.; González-Ferreiro, E. Using low density LiDAR data to map Mediterranean forest characteristics by means of an area-based approach and height threshold analysis. *Rev. Teledetección* **2016**, *2016*, 103–117. [CrossRef]
59. Hayashi, R.; Weiskittel, A.; Sader, S. Assessing the Feasibility of Low-Density LiDAR for Stand Inventory Attribute Predictions in Complex and Managed Forests of Northern Maine, USA. *Forests* **2014**, *5*, 363–383. [CrossRef]
60. Holopainen, M.; Vastaranta, M.; Rasinmäki, J.; Kalliovirta, J.; Mäkinen, A.; Reija, H.; Melkas, T.; Yu, X.; Hyyppä, J.; Hyyppä, H. Estimation of timber assortments using low-density ALS data. In *ISPRS TC VII Symposium–100 Years ISPRS*; Székely, W.W.B., Ed.; IAPRS: Vienna, Austria, 2010; Volume XXXVIII, pp. 59–64.
61. Mehtátalo, L.; Virolainen, A.; Tuomela, J.; Packalen, P. Estimating Tree Height Distribution Using Low-Density ALS Data with and without Training Data. *IEEE J. Sel. Top. Appl. Earth Obs. Remote Sens.* **2015**, *8*, 1432–1441. [CrossRef]
62. Montealegre, A.L.; Lamelas, M.T.; de la Riva, J.; García-Martín, A.; Escribano, F. Use of low point density ALS data to estimate stand-level structural variables in Mediterranean Aleppo pine forest. *Forestry* **2016**, *89*, 373–382. [CrossRef]
63. Næsset, E. Predicting forest stand characteristics with airborne scanning laser using a practical two-stage procedure and field data. *Remote Sens. Environ.* **2002**, *80*, 88–99. [CrossRef]
64. Næsset, E.; Økland, T. Estimating tree height and tree crown properties using airborne scanning laser in a boreal nature reserve. *Remote Sens. Environ.* **2002**, *79*, 105–115. [CrossRef]
65. Holopainen, M.; Vastaranta, M.; Hyyppä, J. Outlook for the Next Generation's Precision Forestry in Finland. *Forests* **2014**, *5*, 1682–1694. [CrossRef]
66. Lin, L.; Hao, Z.; Post, C.J.; Mikhailova, E.A. Protection of Coastal Shelter Forests Using UAVs: Individual Tree and Tree-Height Detection in *Casuarina equisetifolia* L. Forests. *Forests* **2023**, *14*, 233. [CrossRef]
67. Young, D.J.N.; Koontz, M.J.; Weeks, J.M. Optimizing aerial imagery collection and processing parameters for drone-based individual tree mapping in structurally complex conifer forests. *Methods Ecol. Evol.* **2022**, *13*, 1447–1463. [CrossRef]
68. Axelsson, P. DEM Generation from Laser Scanner Data Using Adaptive TIN Models. *ISPRS-Int. Arch. Photogramm. Remote Sens. Spat. Inf. Sci.* **2000**, *33*, 110–117. [CrossRef]
69. Nemmaoui, A.; Aguilar, F.J.; Aguilar, M.A. UAV-Based Digital Terrain Model Generation to Support Accurate Inventories in Mediterranean Forests. In *Advances in Design Engineering III. INGEGRAF 2022. Lecture Notes in Mechanical Engineering*; Cavas-Martínez, F., Marín Granados, M.D., Mirálbes Buil, R., De-Cózar-Macías, O.D., Eds.; Springer International Publishing: Cham, Switzerland, 2023; pp. 565–581. ISBN 978-3-031-20325-1.
70. Torres, F.M.; Tommaselli, A.M.G. A Lightweight UAV-Based Laser Scanning System for Forest Application. *Bol. Ciências Geodésicas* **2018**, *24*, 318–334. [CrossRef]

71. Zhao, X.; Guo, Q.; Su, Y.; Xue, B. Improved progressive TIN densification filtering algorithm for airborne LiDAR data in forested areas. *ISPRS J. Photogramm. Remote Sens.* **2016**, *117*, 79–91. [CrossRef]
72. Montealegre, A.L.; Lamelas, M.T.; Riva, J. de la A Comparison of Open-Source LiDAR Filtering Algorithms in a Mediterranean Forest Environment. *IEEE J. Sel. Top. Appl. Earth Obs. Remote Sens.* **2015**, *8*, 4072–4085. [CrossRef]
73. Lisein, J.; Pierrot-Deseilligny, M.; Bonnet, S.S.; Lejeune, P. A Photogrammetric Workflow for the Creation of a Forest Canopy Height Model from Small Unmanned Aerial System Imagery. *Forests* **2013**, *4*, 922–944. [CrossRef]
74. Roussel, J.R.; Auty, D.; Coops, N.C.; Tompalski, P.; Goodbody, T.R.H.; Meador, A.S.; Bourdon, J.F.; de Boissieu, F.; Achim, A. lidR: An R package for analysis of Airborne Laser Scanning (ALS) data. *Remote Sens. Environ.* **2020**, *251*, 112061. [CrossRef]
75. R Core Team R: The R Project for Statistical Computing. Available online: https://www.r-project.org/ (accessed on 23 December 2022).
76. Zhen, Z.; Quackenbush, L.J.; Zhang, L.; Swatantran, A.; Baghdadi, N.; Thenkabail, P.S. Trends in Automatic Individual Tree Crown Detection and Delineation—Evolution of LiDAR Data. *Remote Sens.* **2016**, *8*, 333. [CrossRef]
77. Xu, X.; Iuricich, F.; De Floriani, L. A topology-based approach to individual tree segmentation from airborne LiDAR data. *Geoinformatica* **2023**, *27*, 759–788. [CrossRef]
78. Dalponte, M.; Coomes, D.A. Tree-centric mapping of forest carbon density from airborne laser scanning and hyperspectral data. *Methods Ecol. Evol.* **2016**, *7*, 1236–1245. [CrossRef]
79. Roussel, J.R.; Caspersen, J.; Béland, M.; Thomas, S.; Achim, A. Removing bias from LiDAR-based estimates of canopy height: Accounting for the effects of pulse density and footprint size. *Remote Sens. Environ.* **2017**, *198*, 1–16. [CrossRef]
80. Véga, C.; Renaud, J.P.; Durrieu, S.; Bouvier, M. On the interest of penetration depth, canopy area and volume metrics to improve Lidar-based models of forest parameters. *Remote Sens. Environ.* **2016**, *175*, 32–42. [CrossRef]
81. Baltsavias, E. Airborne laser scanning: Basic relations and formulas. *ISPRS J. Photogramm. Remote Sens.* **1999**, *54*, 199–214. [CrossRef]
82. Khosravipour, A.; Skidmore, A.K.; Isenburg, M.; Wang, T.; Hussin, Y.A. Generating pit—Free canopy height models from airborne lidar. *Photogramm. Eng. Remote Sens. PE&RS* **2014**, *80*, 863–872. [CrossRef]
83. Persson, Å.; Holmgren, J.; Söderman, U. Detecting and measuring individual trees using an airborne laser scanner. *Photogramm. Eng. Remote Sens.* **2002**, *68*, 925–932.
84. Leckie, D.; Gougeon, F.; Hill, D.; Quinn, R.; Armstrong, L.; Shreenan, R. Combined high-density lidar and multispectral imagery for individual tree crown analysis. *Can. J. Remote Sens.* **2014**, *29*, 633–649. [CrossRef]
85. Parkan, M. Digital Forestry Toolbox for Matlab/Octave. Available online: http://mparkan.github.io/Digital-Forestry-Toolbox/ (accessed on 23 November 2020).
86. Bartier, P.M.; Keller, C.P. Multivariate interpolation to incorporate thematic surface data using inverse distance weighting (IDW). *Comput. Geosci.* **1996**, *22*, 795–799. [CrossRef]
87. Mohan, M.; de Mendonça, B.A.F.; Silva, C.A.; Klauberg, C.; de Saboya Ribeiro, A.S.; de Araújo, E.J.G.; Monte, M.A.; Cardil, A. Optimizing individual tree detection accuracy and measuring forest uniformity in coconut (*Cocos nucifera* L.) plantations using airborne laser scanning. *Ecol. Modell.* **2019**, *409*, 108736. [CrossRef]
88. Wulder, M.; Niemann, K.O.; Goodenough, D.G. Error reduction methods for local maximum filtering of high spatial resolution imagery for locating trees. *Can. J. Remote Sens.* **2002**, *28*, 621–628. [CrossRef]
89. Wulder, M.; Niemann, K.O.; Goodenough, D.G. Local Maximum Filtering for the Extraction of Tree Locations and Basal Area from High Spatial Resolution Imagery. *Remote Sens. Environ.* **2000**, *73*, 103–114. [CrossRef]
90. Popescu, S.C.; Wynne, R.H. Seeing the trees in the forest: Using lidar and multispectral data fusion with local filtering and variable window size for estimating tree height. *Photogramm. Eng. Remote Sens.* **2004**, *70*, 589–604. [CrossRef]
91. UNFCCC. *Report of the Conference of the Parties Serving as the Meeting of the Parties to the Kyoto Protocol on Its First Session, Held at Montreal from 28 November to 10 December 2005. Addendum. Part Two*; United Nations ClimateChage: Bonn, Germany, 2005.
92. Aurenhammer, F.; Klein, R. Voronoi Diagrams. In *Handbook of Computational Geometry*; Sack, J.-R., Urrutia, J., Eds.; North-Holland: Hagen, Germany, 2000; pp. 201–290. ISBN 978-0-444-82537-7.
93. Bottai, L.; Arcidiaco, L.; Chiesi, M.; Maselli, F. Application of a single-tree identification algorithm to LiDAR data for the simulation of stem volume current annual increment. *J. Appl. Remote Sens.* **2013**, *7*, 073699. [CrossRef]
94. Li, W.; Guo, Q.; Jakubowski, M.K.; Kelly, M. A New Method for Segmenting Individual Trees from the Lidar Point Cloud. *Photogramm. Eng. Remote Sens.* **2012**, *78*, 75–84. [CrossRef]
95. Fischler, M.A.; Bolles, R.C. Random sample consensus. *Commun. ACM* **1981**, *24*, 381–395. [CrossRef]
96. Vauhkonen, J.; Korpela, I.; Maltamo, M.; Tokola, T. Imputation of single-tree attributes using airborne laser scanning-based height, intensity, and alpha shape metrics. *Remote Sens. Environ.* **2010**, *114*, 1263–1276. [CrossRef]
97. Swayze, N.C.; Tinkham, W.T.; Vogeler, J.C.; Hudak, A.T. Influence of flight parameters on UAS-based monitoring of tree height, diameter, and density. *Remote Sens. Environ.* **2021**, *263*, 112540. [CrossRef]
98. Creasy, M.B.; Tinkham, W.T.; Hoffman, C.M.; Vogeler, J.C. Potential for individual tree monitoring in ponderosa pine dominated forests using unmanned aerial system structure from motion point clouds. *Can. J. For. Res.* **2021**, *51*, 1093–1105. [CrossRef]
99. Sokolova, M.; Japkowicz, N.; Szpakowicz, S. Beyond accuracy, F-score and ROC: A family of discriminant measures for performance evaluation. *AAAI Work.-Tech. Rep.* **2006**, *WS-06-06*, 24–29.
100. Goutte, C.; Gaussier, E. A Probabilistic Interpretation of Precision, Recall and F-Score, with Implication for Evaluation. *Lect. Notes Comput. Sci.* **2005**, *3408*, 345–359. [CrossRef]

101. Asner, G.P.; Heidebrecht, K.B. Spectral unmixing of vegetation, soil and dry carbon cover in arid regions: Comparing multispectral and hyperspectral observations. *Int. J. Remote Sens.* **2002**, *23*, 3939–3958. [CrossRef]
102. Wulder, M.A.; Dechka, J.A.; Gillis, M.A.; Luther, J.E.; Hall, R.J.; Beaudoin, A.; Franklin, S.E. Operational mapping of the land cover of the forested area of Canada with Landsat data: EOSD land cover program. *For. Chron.* **2003**, *79*, 1075–1083. [CrossRef]
103. Hyyppä, J.; Hyyppä, H.; Leckie, D.; Gougeon, F.; Yu, X.; Maltamo, M. Review of methods of small-footprint airborne laser scanning for extracting forest inventory data in boreal forests. *Int. J. Remote Sens.* **2008**, *29*, 1339–1366. [CrossRef]
104. Mohan, M.; Silva, C.A.; Klauberg, C.; Jat, P.; Catts, G.; Cardil, A.; Hudak, A.T.; Dia, M. Individual Tree Detection from Unmanned Aerial Vehicle (UAV) Derived Canopy Height Model in an Open Canopy Mixed Conifer Forest. *Forests* **2017**, *8*, 340. [CrossRef]
105. Belmonte, A.; Sankey, T.; Biederman, J.A.; Bradford, J.; Goetz, S.J.; Kolb, T.; Woolley, T. UAV-derived estimates of forest structure to inform ponderosa pine forest restoration. *Remote Sens. Ecol. Conserv.* **2020**, *6*, 181–197. [CrossRef]
106. Tinkham, W.T.; Swayze, N.C. Influence of Agisoft Metashape Parameters on UAS Structure from Motion Individual Tree Detection from Canopy Height Models. *Forests* **2021**, *12*, 250. [CrossRef]
107. Hauglin, M.; Næsset, E. Detection and Segmentation of Small Trees in the Forest-Tundra Ecotone Using Airborne Laser Scanning. *Remote Sens.* **2016**, *8*, 407. [CrossRef]
108. Véga, C.; Durrieu, S. Multi-level filtering segmentation to measure individual tree parameters based on Lidar data: Application to a mountainous forest with heterogeneous stands. *Int. J. Appl. Earth Obs. Geoinf.* **2011**, *13*, 646–656. [CrossRef]
109. Gaveau, D.L.A.; Hill, R.A. Quantifying canopy height underestimation by laser pulse penetration in small-footprint airborne laser scanning data. *Can. J. Remote Sens.* **2014**, *29*, 650–657. [CrossRef]
110. Westoby, M.J.; Brasington, J.; Glasser, N.F.; Hambrey, M.J.; Reynolds, J.M. 'Structure-from-Motion' photogrammetry: A low-cost, effective tool for geoscience applications. *Geomorphology* **2012**, *179*, 300–314. [CrossRef]
111. Ferraz, A.; Bretar, F.; Jacquemoud, S.; Gonçalves, G.; Pereira, L.; Tomé, M.; Soares, P. 3-D mapping of a multi-layered Mediterranean forest using ALS data. *Remote Sens. Environ.* **2012**, *121*, 210–223. [CrossRef]
112. Xu, S.; Sun, X.; Yun, J.; Wang, H. A New Clustering-Based Framework to the Stem Estimation and Growth Fitting of Street Trees from Mobile Laser Scanning Data. *IEEE J. Sel. Top. Appl. Earth Obs. Remote Sens.* **2020**, *13*, 3240–3250. [CrossRef]
113. Dalponte, M. Package 'itcSegment': Individual Tree Crowns Segmentation. R Package Version 0.6. 2017. Available online: https://CRAN.R-project.org/package=itcSegment (accessed on 1 March 2017).
114. Jucker, T.; Caspersen, J.; Chave, J.; Antin, C.; Barbier, N.; Bongers, F.; Dalponte, M.; van Ewijk, K.Y.; Forrester, D.I.; Haeni, M.; et al. Allometric equations for integrating remote sensing imagery into forest monitoring programmes. *Glob. Chang. Biol.* **2017**, *23*, 177–190. [CrossRef]
115. Montero, G.; Ruiz-Peinado, R.; Muñoz, M. *Producción de Biomasa y Fijación de CO_2 por los Bosques Españoles*; Monografías I.N.I.A.: Forestal; Ministerio de Educación y Ciencia; Instituto Nacional de Investigación y Tecnología Agraria y Alimentaria: Madrid, Spain, 2005; ISBN 9788474985122.
116. Spanish Forest Map. Available online: https://www.miteco.gob.es/es/biodiversidad/servicios/banco-datos-naturaleza/informacion-disponible/mfe50.html (accessed on 3 April 2022).

Disclaimer/Publisher's Note: The statements, opinions and data contained in all publications are solely those of the individual author(s) and contributor(s) and not of MDPI and/or the editor(s). MDPI and/or the editor(s) disclaim responsibility for any injury to people or property resulting from any ideas, methods, instructions or products referred to in the content.